Additive Manufacturing Letters 14 (2025) 100304

Contents lists available at ScienceDirect

Additive Manufacturing Letters

journal homepage: www.elsevier.com/locate/addlet

Short review

Towards fully 3D printed dielectric elastomer actuators—A mini review

Rollo Pattinson [a,*], Nathan Ellmer [b,*], Mokarram Hossain [b], Rogelio Ortigosa [c], Jesús Martínez-Frutos [c], Antonio J. Gil [b,*], Anil Bastola [a,*]

[a] Materials and Manufacturing Research Institute, Faculty of Science and Engineering, Swansea University, Bay Campus, SA1 8EN, United Kingdom
[b] Zienkiewicz Institute for Modelling, Data and AI, Faculty of Science and Engineering, Swansea University, Bay Campus, SA1 8EN, United Kingdom
[c] Technical University of Cartagena, Campus Muralla del Mar, Cartagena, 30202 Murcia, Spain

ARTICLE INFO

Keywords:
Dielectric elastomer actuators
Additive manufacturing
Topology optimisation
Electro-active polymers

ABSTRACT

Dielectric elastomer actuators (DEAs) have attracted the interest of researchers in soft robotics and biomimetics, due to their versatile capabilities, explored through numerical analysis and experimentation. Advances in computational simulation techniques have accelerated numerical studies on DEAs, enabling even design optimisation for improved performance. However, as computational models grow in sophistication, the fabrication methods required often exceed the capabilities of traditional manufacturing. Additive manufacturing, in particular 3D printing, offers a promising solution to the challenges of realising intricate multi-functional designs developed through topology optimisation. Its precision and ability to create complex geometries make it well-suited for translating computational designs into functional DEA devices. This mini-review examines recent progress in 3D printing for DEA fabrication, emphasising its role in bridging the gap between computational design and physical devices. It also highlights emerging technologies and key challenges that must be addressed to fully realise topologically optimised DEA designs.

1. Introduction

Dielectric elastomer actuators (DEAs) are multi-material systems which form a subclass of electroactive polymers (EAPs). This promising technology showcases the opportunity to exploit their inherent flexibility, light weight nature, and high energy density [1], across a wide range of applications. Suitable fields include soft robotics [2], healthcare [3], and adaptive optics [4,5], just to name a few.

DEAs are comprised of two primary components — a dielectric elastomer film and a flexible conductive layer, often referred to as compliant electrode [6]. Upon application of a high voltage (1–10 kV see Table 2), the generated electrostatic force tends to compress the elastomer in thickness, yielding in-plane expansion (due to the elastomers near-incompressibility), thus resulting in mechanical actuation as shown in Fig. 1(a). Design parameters such as elastomer film thickness, magnitude of applied pre-stretch, and geometry of electrodes have significant influence over the overall performance and responsiveness of DEAs [7]. In conjunction with the two primary components, many DEAs implement additional components such as rigid frames [8–10] to facilitate and maintain pre-stretching, or passive layers [11,12] and fibres [13,14] to influence the actuation direction and performance.

The first conceptualisation of DEAs can be traced to the derivation of the Maxwell equations which demonstrated that electric fields induce mechanical stress [27]. As a result, this led to Röntgen to study the electro-mechanical effects of electric charges sprayed onto a natural rubber in 1880 [16], introducing the fundamental mechanism for the operation of DEAs. In 1958, the artificial muscle was devised by Gaylord [17], which was originally driven by pneumatics. This concept played a significant role in demonstrating the possibilities of soft actuators in the field of orthotics [18]. However, it took until the late 1990s to begin research on the first DEAs, as published by Pelrine et al. in 2000 [20,28]. By 2010, Brochu et al. [29] had compiled a comprehensive review showcasing DEA device development. It is important to emphasise that the majority of materials being used for DEAs were commercially produced and intended for unrelated applications, thus highlighting the need for advanced material development. Around this time, there were also significant advancements in DEAs with the capability of self-sensing [21] and self-healing [23]. By the 2010s more complex designs were being considered which required increasing levels of detail from the manufacturing standpoint. At this time - and still to this day, 3D Printing (3DP) is widely seen as the solution to the fabrication of these more intricate designs due to the ability to realise complex geometries [30]. To the best of the authors' knowledge, the first DEA was printed using an aerosol jet technique in

* Corresponding authors.
E-mail addresses: r.w.j.pattinson@swansea.ac.uk (R. Pattinson), n.s.ellmer@swansea.ac.uk (N. Ellmer), a.j.gil@swansea.ac.uk (A.J. Gil), a.k.bastola@swansea.ac.uk (A. Bastola).

https://doi.org/10.1016/j.addlet.2025.100304
Received 19 March 2025; Received in revised form 25 June 2025; Accepted 13 July 2025
Available online 25 July 2025

Acronyms

2PP	Two Photon Polymerisation
3DP	3D Printing
AM	Additive Manufacturing
CAD	Computer Aided Design
DEA	Dielectric Elastomer Actuator
DEF	Dielectric Elastomer Fibres
DIW	Direct Ink Writing
DLP	Digital Light Processing
EAP	Electro-Active Polymer
EHD	Electrohydrodynamic
HDEA	Helical Dielectric Elastomer Actuators
FDM	Fused Deposition Modelling
PDMS	Polydimethylsiloxane
SIMP	Solid Isotropic Material with Penalisation
SLA	Stereolithography Apparatus
TPE	Thermoplastic Elastomer
TPU	Thermoplastic Polyurethane
VP	Vat Polymerisation

2013 [22], and by the 2020s a variety of other 3DP techniques were explored in order to address more sophisticated designs [24–26].

Conventional DEA fabrication typically involves casting of two-part silicones and/or pre-stretching prefabricated elastomers for the dielectric layer. Example materials include silicone-based elastomers such as PDMS (polydimethylsiloxane) or acrylic elastomers such as VHB (3M). For ease of fabrication, conductive layers have commonly been painted on using carbon grease [29]. Alternatively, materials such as carbon nanotubes, or other metallic, and conductive nanostructures can be embedded into an elastomeric matrix. Although these methods yield highly efficient DEAs, they are often constrained by labour-intensive processes, challenges in achieving miniaturisation, and integration into complex systems — all of which can be bypassed through manufacturing using 3D printers [31,32]. Fig. 1(b) shows the growth in interest of 3DP in the field of DEAs but also highlights the sparsity in comparison to overall DEA research. As of today, the realisation of fully 3D printed DEAs still presents significant challenges that must be addressed to unlock their full potential. Whilst 3DP offers unparallelled design freedom and the ability to put forward complex design geometries, the significance of dielectric, conductive and mechanical properties must be weighed against the desired properties for printing [33].

The range of applications for DEAs is becoming vast as the capability to realise increasingly sophisticated devices becomes more accessible. Soft robotics is a particularly attractive field for DEAs due to their flexibility and high energy density — low weight high power output [1]. A significant advantage of these materials which can be exploited through soft robotics is their ability to replicate biological designs, thus enabling biomimetic devices. Examples include walking/crawling propulsion as demonstrated by Ji et al. [34] with untethered insect inspired robots, or flying robots as developed by Chen et al. [35] to produce a controllable aerial microrobot. Aquatic based robots have also been explored by Tang et al. [36] in the form of a frog-inspired swimming robot or Shintake et al. [37] with a jellyfish inspired actuator. Additionally, extensive research has been conducted in the field of humanoid robotics due to DEAs having similar properties to that of natural muscle with respect to strain, energy density and response time [38]. This has also opened up possibilities in healthcare with the potential for prosthetics and artificial muscles [38]. Another example application for DEAs is for use in tuneable lens systems whereby an actuator is used to adjust the focal length [39,40]. This requires transparent dielectric materials such as Sylgard 184 (DOW) as well as transparent electrodes. Shian et al. [39] have explored the development of transparent electrodes enabling lens devices capable of 100% focal length adjustments [40]. As well as tuning optics, DEAs have also been explored for use in tuning acoustic properties, with local resonators, termed phononic crystals [41] which can be used to control sound propagation by isolating waves. Not only can this influence the acoustic properties of materials, but it has also been shown to improve resistance to fracture in the material [42,43]. Shrestha et al. [44,45] demonstrates a bio-inspired acoustic absorber based on a DEA that mimics the blooming of flower petals. Furthermore, DEA devices provide an excellent opportunity to develop increasingly intricate tactile displays or interfaces. Capable of actuating and sensing [21], DEAs can be implemented into wearable devices providing haptic feedback thus enabling improved accessibility. For example Qu et al. [46] presents Braille displays for people affected by vision impairments. Ji et al. [47] have also demonstrated this technology in order to enable the sensing of virtual objects within a virtual reality environment. It is also important to note that these materials have the ability to function as soft dielectric sensors and generators following similar principles as DEAs [48]. Whilst this functionality is not discussed in this work, it also highlights the scale of potential use cases for DEAs.

To showcase the importance of developing 3DP techniques for the manufacturing of DEAs, it is essential to first demonstrate the progression in in-silico design and hence the range of possibilities that aim to be manufacturable. Therefore, this mini review will begin by briefly describing the progression of Topology Optimisation (TO) techniques, followed by presenting the use of 3DP to realise these designs including examples of current single component and fully 3D printed DEA devices. The key challenges associated with materials, processes and actuation will also be highlighted before providing a final summary and outlook for the future of research in the field of 3DP DEA devices.

2. Progress in In-silico DEA design

2.1. Governing equations

In-silico modelling forms an integral part of device design to ensure the likelihood of manufacturing success and simultaneously reduce the need of inefficient trial-and-error. To model the response of a DEA, a framework for modelling coupled physics must be used. The set of strong form equations (typically displayed in a Lagrangian framework) used to model the so-called boundary value problem consists of the conservation of linear momentum and simplified Maxwell's equations as (see the Eq. (1) in Box I). where $\mathcal{B}_0$ denotes the undeformed domain and the ∇_0 operator represents the gradient with respect to the undeformed material coordinates $\boldsymbol{X} \in \mathcal{B}_0$. The mapping $\boldsymbol{\phi} : \mathcal{B}_0 \to \mathcal{B}$ describes the relationship between the undeformed $\mathcal{B}_0$ and deformed $\mathcal{B}$ domains which leads to the definition of the deformation gradient tensor or fibre map $\boldsymbol{F}$. Additional mechanical quantities include the first Piola–Kirchhoff stress tensor $\boldsymbol{P}$ as well as the forces acting per unit undeformed volume $\boldsymbol{f}_0$ and per unit undeformed surface area $\boldsymbol{t}_0$. For the electrostatics, φ denotes the electric potential field which leads to the definition of the material electric field $\boldsymbol{E}_0$. The other electrostatic quantities include the material electric displacement $\boldsymbol{D}_0$ as well as the electric charge per unit undeformed volume ρ_0 and per unit undeformed area ω_0. Furthermore, $\boldsymbol{N}$ denotes the outward pointing normal acting on the boundary which is split into two parts corresponding to the application of the Dirichlet $\{\partial_{\boldsymbol{\phi}}\mathcal{B}_0, \partial_{\varphi}\mathcal{B}_0\}$ and Neumann $\{\partial_{\boldsymbol{t}}\mathcal{B}_0, \partial_{\omega}\mathcal{B}_0\}$ boundary conditions such that

$$\underbrace{\begin{aligned}\partial\mathcal{B}_0 &= \partial_{\boldsymbol{\phi}}\mathcal{B}_0 \cup \partial_{\boldsymbol{t}}\mathcal{B}_0,\\ \emptyset &= \partial_{\boldsymbol{\phi}}\mathcal{B}_0 \cap \partial_{\boldsymbol{t}}\mathcal{B}_0,\end{aligned}}_{\text{Mechanical boundary regions}} \qquad \underbrace{\begin{aligned}\partial\mathcal{B}_0 &= \partial_{\varphi}\mathcal{B}_0 \cup \partial_{\omega}\mathcal{B}_0,\\ \emptyset &= \partial_{\varphi}\mathcal{B}_0 \cap \partial_{\omega}\mathcal{B}_0.\end{aligned}}_{\text{Electrostatic boundary regions}} \tag{2}$$

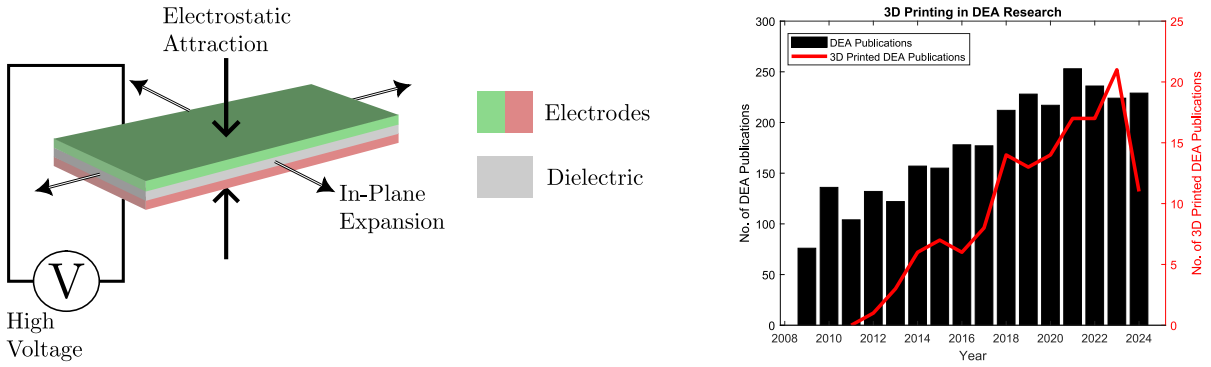

(a) (b)

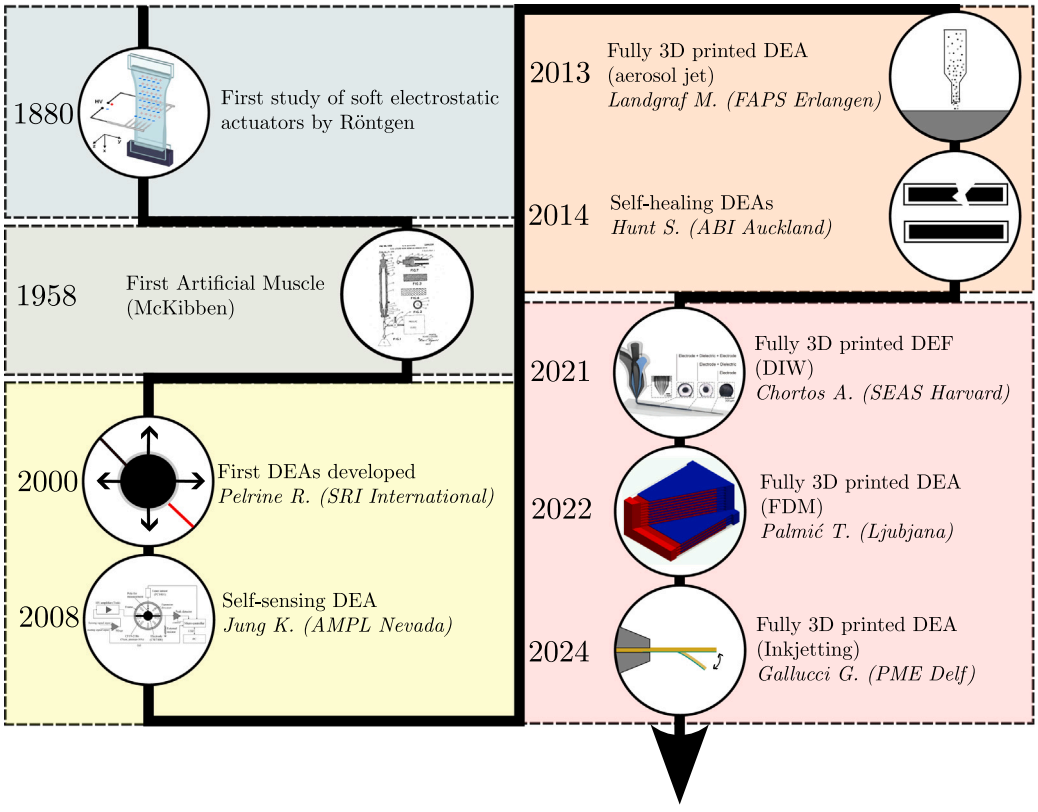

(c)

Fig. 1. (a) Presets the mechanism of DEA actuation. (b) Demonstrates the number of DEA articles (black bars) and the number which included AM (red line) by publication year. Data obtained from [15]. (c) Displays a timeline of DEA development. From start to present; Röntgen's actuator (image reproduced from [16]), McKibben artificial muscle [17–19], Pelrine et al. [20] high strain DEAs, Jung et al. [21] self-sensing DEA (image reproduced from [21]), Landgraf et al. [22] aerosol jet printed DEA, Hunt et al. [23] self-healing DEA, Chortos et al. [24] fully printed dielectric fibre (image reproduced from [24]), Palmić et al. multi-layer FDM printed DEA. (image reproduced from [25]), Gallucci et al. fully inkjet printed DEA [26].

$$
\begin{aligned}
\boldsymbol{F} &= \nabla_0 \boldsymbol{\phi}, && \text{in } \mathcal{B}_0 \\
\mathrm{DIV}\boldsymbol{P} &= -\boldsymbol{f}_0, && \text{in } \mathcal{B}_0 \\
\boldsymbol{\phi} &= \boldsymbol{\phi}^*, && \text{on } \partial_{\boldsymbol{\phi}}\mathcal{B}_0 \\
\boldsymbol{P}\boldsymbol{N} &= \boldsymbol{t}_0, && \text{on } \partial_t\mathcal{B}_0
\end{aligned}
\qquad
\begin{aligned}
\boldsymbol{E}_0 &= -\nabla_0 \varphi, && \text{in } \mathcal{B}_0 \\
\mathrm{DIV}\boldsymbol{D}_0 &= \rho_0, && \text{in } \mathcal{B}_0 \\
\varphi &= \varphi^*, && \text{on } \partial_{\varphi}\mathcal{B}_0 \\
\boldsymbol{D}_0 \cdot \boldsymbol{N} &= -\omega_0, && \text{on } \partial_{\omega}\mathcal{B}_0
\end{aligned}
\tag{1}
$$

Conservation of linear momentum and kinematics — Gauss' and Faraday's Law

Box I.

2.2. Internal and free energy densities

To obtain definitions for both $\boldsymbol{P}$ and $\boldsymbol{D}_0$, a constitutive relation is required — typically in the form of a free energy density. The Helmholtz free energy density $\Psi\left(\boldsymbol{F}, \boldsymbol{E}_0\right)$ allows for the definitions of $\boldsymbol{P}$ and $\boldsymbol{D}_0$ as follows

$$\boldsymbol{P} = \partial_{\boldsymbol{F}}\Psi\left(\boldsymbol{F}, \boldsymbol{E}_0\right), \qquad \boldsymbol{D}_0 = -\partial_{\boldsymbol{E}_0}\Psi\left(\boldsymbol{F}, \boldsymbol{E}_0\right). \tag{3}$$

where $\partial_{\boldsymbol{\mathcal{X}}}(\bullet)$ denotes the partial derivative of the field $(\bullet)$ with respect to $\boldsymbol{\mathcal{X}}$. Alternatively, it is also possible to obtain $\boldsymbol{E}_0$ in terms of $\boldsymbol{F}$ and $\boldsymbol{D}_0$ through the internal energy density $e\left(\boldsymbol{F}, \boldsymbol{D}_0\right)$ that can be obtained via the Legendre transform as

$$e\left(\boldsymbol{F}, \boldsymbol{D}_0\right) = \Psi\left(\boldsymbol{F}, \boldsymbol{E}_0\left(\boldsymbol{F}, \boldsymbol{D}_0\right)\right) + \boldsymbol{D}_0 \cdot \boldsymbol{E}_0\left(\boldsymbol{F}, \boldsymbol{D}_0\right), \tag{4}$$

where the definitions of $\boldsymbol{P}$ and $\boldsymbol{D}_0$ can then be consistently expressed through

$$\boldsymbol{P} = \partial_{\boldsymbol{F}} e\left(\boldsymbol{F}, \boldsymbol{D}_0\right), \qquad \boldsymbol{E}_0 = \partial_{\boldsymbol{D}_0} e\left(\boldsymbol{F}, \boldsymbol{D}_0\right). \tag{5}$$

Once an appropriate free energy density has been chosen, then one can consider the procedure to multi-scale composite modelling — required to capture laminations or inclusions occurring at the microscale. This requires the consideration of two new parameters $\{\boldsymbol{\alpha}, \boldsymbol{\beta}\}$ which refer to the microfluctuations in the deformation and electric potential fields. To get the homogenised effective energy from a combination of two or more material models the following minimisation must take place

$$e\left(\boldsymbol{F}, \boldsymbol{D}_0\right) = \arg\min_{\boldsymbol{\alpha},\boldsymbol{\beta}} \left\{\hat{e}\left(\boldsymbol{F}, \boldsymbol{D}_0, \boldsymbol{\alpha}, \boldsymbol{\beta}\right)\right\}, \tag{6}$$

where

$$\begin{aligned}\hat{e}\left(\boldsymbol{F}, \boldsymbol{D}_0, \boldsymbol{\alpha}, \boldsymbol{\beta}\right) = {} & c^a e^a\left(\boldsymbol{F}^a\left(\boldsymbol{F}, \boldsymbol{\alpha}\right), \boldsymbol{D}_0^a\left(\boldsymbol{D}_0, \boldsymbol{\beta}\right)\right) \\ & + c^b e^b\left(\boldsymbol{F}^b\left(\boldsymbol{F}, \boldsymbol{\alpha}\right), \boldsymbol{D}_0^b\left(\boldsymbol{D}_0, \boldsymbol{\beta}\right)\right),\end{aligned} \tag{7}$$

wherein the homogenised energy is comprised of two contributions parts, a and b, with volume fractions c^a and c^b, respectively. This minimisation is commonly associated with rank-n homogenisation theory [49,50], but has been seen to be simply extended to Representative Volume Elements in the context of a FEM^2 approach [51].

2.3. Topology optimisation for DEAs

DEAs with sophisticated deformation and actuation modes, thereby unlocking the potential for unlimited degree of freedom soft actuators, need to be designed to produce either an inhomogeneous activating electric field – thus activating selected regions sandwiched between electrodes [52,53], or designed to have inhomogeneous material properties – yielding increased activation in regions of reduced stiffness or increased dielectric permittivity [54–56]. Achieving either of these is not a trivial undertaking and TO is required to obtain these often intricate designs. Prior to considering the objective function it is important to state that the optimisation will work on a distribution of active to passive material (electrode optimisation) or the distribution of multiple materials and hence their respective properties (multi-material optimisation). Similarly to the homogenisation procedure, the free (internal) energy definition can be decomposed at any location into its components from either the passive and active materials of each material itself via

$$\begin{aligned}e\left(\boldsymbol{F}, \boldsymbol{D}_0, \eta\left(\boldsymbol{X}\right)\right) = {} & \left(\eta\left(\boldsymbol{X}\right)\right)^p e^{active}\left(\boldsymbol{F}, \boldsymbol{D}_0\right) \\ & + \left[1 - \left(\eta\left(\boldsymbol{X}\right)\right)^p\right] e^{passive}\left(\boldsymbol{F}, \boldsymbol{D}_0\right),\end{aligned} \tag{8}$$

where the function $\left(\eta\left(\boldsymbol{X}\right)\right)^p$ is a method specific function – with a carefully selected exponent p – which interpolates between the active and passive materials. The selection of $\eta\left(\boldsymbol{X}\right)$ is crucial in achieving a smooth interpolation which is differentiable. Having defined the homogenised energy, the optimisation problem P can now be laid out

$$P\begin{cases}\arg\min_{\eta(\boldsymbol{X})} \mathcal{J}\left(\boldsymbol{\phi}\left(\boldsymbol{X}\right)\right), \\ \text{s.t}\begin{cases}\text{Governing equations}, \\ \text{Constitutive model}, \\ 0 \le \eta\left(\boldsymbol{X}\right) \le 1,\end{cases}\end{cases} \tag{9}$$

where $\mathcal{J}\left(\boldsymbol{\phi}\left(\boldsymbol{X}\right)\right)$ is the objective function. An example of an objective function with a target deformation $\bar{\boldsymbol{\phi}}\left(\boldsymbol{X}\right)$ as seen in [56] is

$$\mathcal{J}\left(\boldsymbol{\phi}\left(\boldsymbol{X}\right)\right) = \frac{1}{2}\int_{\mathcal{B}_0} \left\|\boldsymbol{\phi}\left(\boldsymbol{X}\right) - \bar{\boldsymbol{\phi}}\left(\boldsymbol{X}\right)\right\|^2 dV. \tag{10}$$

This objective function was used for a phase-field type procedure and other processes may require it to be altered. The interested reader is directed to the beginning of this subsection where references to other techniques have been highlighted. Moreover, thus far the description has been generic and can be applied to both the optimisation of electrode placement and multi-material distribution. The remainder of this section will outline the variety of TO techniques implemented in the literature.

2.3.1. Electrode placement

Designing complex deformations through selectively placing electrodes [52] (presented in Fig. 2(a)–(c)) or stiffeners (presented in Fig. 2(d)–(f)) [54] is not necessarily a straightforward process and requires sometimes abstract designs such as those produced in works by Ortigosa et al. [55–58]. To obtain these often-unthinkable designs requires the application of mathematical TO techniques. Several approaches to TO are available such as the Solid Isotropic Material with Penalisation (SIMP) [59], level-set [60,61], and phase-field methods [62,63]. Detailed explanations of these approaches are out of the scope for this review and the interested reader is referred to their associated references.

The precise design and positioning of electrodes in order to induce an inhomogeneous electric field has been investigated experimentally by Rossiter et al. [64] to obtain rotations, and by Clarke et al. [52] to yield complex morphing. There now exists several works which attempt to replicate, enhance, and extend these demonstrated deformations utilising computational frameworks in combination with the aforementioned TO techniques. Wang et al. [65] displayed a number of examples which employed a Bezier curve TO method to maximise the rotation angle induced by the applied inhomogeneous electric field. Using a level-set TO approach, Chen et al. [66] showcased simulation results which maximised the displacement in a given direction at specified locations. This was then presented alongside experimental results which used this maximised actuation to transform a planform shape into a 3D sculpture. More recently, Ortigosa et al. [67] have employed the SIMP method to maximise the achievable actuation through the optimisation of a compliance type objective function. A number of numerical examples using TO, including complex bending and torsional actuators were presented with non-trivial active component designs. Additionally, Ortigosa et al. [57] has introduced a multi-resolution approach which enables a finer resolution for modelling the application of the electrodes without needing to increase the resolution of the entire domain to solve for standard quantities such as displacements, thus rendering high resolution solutions with reasonable computational cost.

2.3.2. Dielectric material variation

Multi-material approaches to producing sophisticated deformations have also been experimentally explored by Clarke's research group at Harvard [54,68] where the introduction of stiffening elements is shown to induce designed morphing. This design approach has been far less extensively researched for TO in the context of DEAs. Employing a phase-field TO method, Ortigosa et al. [55] showcased an impressive array of intricate designs attainable through TO, mimicking the

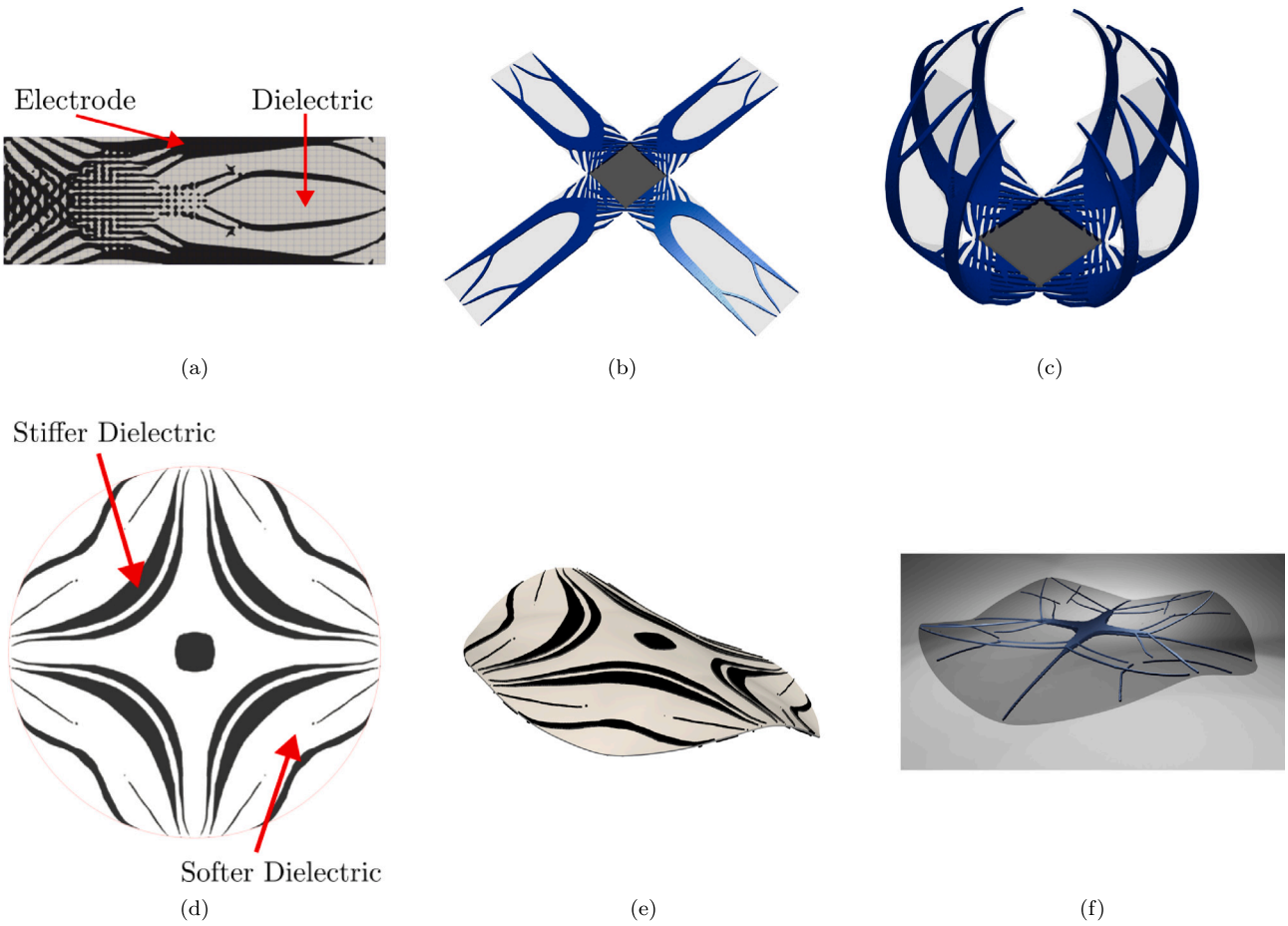

Fig. 2. (a)–(c) Examples of complex electrode placement generated via TO, where electrodes are represented by black (image (a)) and dark blue (images (b) and (c)) regions. (a) Electrode design via TO. (b) Undeformed configuration with the electrode placement. (c) Deformed configuration due to inhomogeneous electric field. Images (a)–(c) reproduced from [57]. (d)–(f) Examples of stiffeners and multi-material designs generated via TO, where the stiffer material is represented by the black regions. (d) Stiffener design. (e) Deformed configuration with the stiffeners. (f) Deformed configuration due to stiffeners in an alternate layout. Images (d)–(f) reproduced from [55].

dome design from Clarke et al. [54] and to further explore complex multi-directional bending examples. Alternatively, Ref. [56] has also demonstrated that instead of simply adding stiffeners, an array of multiple materials could be optimally positioned throughout the device in such a way that an inhomogeneous distribution of material properties leads to the desirable deformation under a uniform electric field. Moreover, whilst not for maximising displacements, multi-material TO has been applied by Sharma et al. [41] using a gradient method to alter the distribution of fibre materials within a matrix, thus tuning the respective band gap characteristics. In doing so bespoke phononic devices can be designed with maximum band gaps between adjacent bands enabling enhanced control over wave propagation.

2.4. Current design and fabrication of topologically optimised DEAs

TO has been demonstrated to have the capability to accelerate complex device design when there is an objective or target deformation. Furthermore, TO can reduce resource wastage due to negating the need for experimental trial and error approaches. 3DP is widely accepted as the approach to realise complex designs such as those developed through TO, however, with the intricacies of emerging TO designs (e.g. [55,56]), it is important to assess and enhance the printing capability to align with the progression in resolution from computational techniques. Moreover, constraints need to be provided to circumvent the TO solution producing impracticable designs such as a vast number of electrodes, positioned more centrally adding difficulty to provide power and thus control. Consequently, actuation limitations need to be assessed and added as feature constraints within TO processes. Furthermore, to the time of publication, there is no knowledge of TO incorporating viscous effects – which when developing custom 3D printable feedstock will certainly have a major presence.

Realising TO designs through 3DP is critical since the techniques can overcome geometric constraints and allows for the fabrication of complex bespoke geometries but more importantly, it allows for the integration of multiple materials. Moreover, 3DP technology opens the door for gradient materials which would further reduce TO design constraints with respect to selecting a specific material. This is pivotal for the development of a sophisticated customised fully 3D printed DEA devices consisting of both the designed conductive and dielectric layers.

3. Progress in 3D printing of DEAs

Whilst 3DP remains uncommon in the field of DEAs – representing only 5.6% of published articles in 2023 [15] – considerable progress has been made over the past decade since the publication of the first articles.

Table 1 presents an overview of characteristics for the variety of 3DP types which can be used to fabricate DEAs. This is accompanied by Fig. 3 which provides a visual representation for each technique. This section will now first discuss 3DP of a single DEA component, namely either the conductive or dielectric layer, followed by examples of fully 3D printed multi-material DEA devices.

Table 1
The key characteristics of 3DP methods that are suitable for manufacturing DEAs.

Method	Technique	Feedstock	Requirements	Resolution	Multi-material
Extrusion	DIW	Ink	Thermal/UV	5–200 μm [33]	Yes
	FDM	Filament	Thermoplastic	50–200 μm [33]	Yes
Vat polymerisation	SLA	Resin	UV curable	0.6–2 μm [69]	Limited
	DLP	Resin	UV curable	0.6–2 μm [69]	Limited
	2PP	Resin	UV curable	≤100 nm [70]	Limited
Material jetting	Low viscosity	Ink	Thermal/UV	≤100 μm [71]	Yes
	High viscosity	Ink	Thermal/UV	300–350 μm [72]	Yes

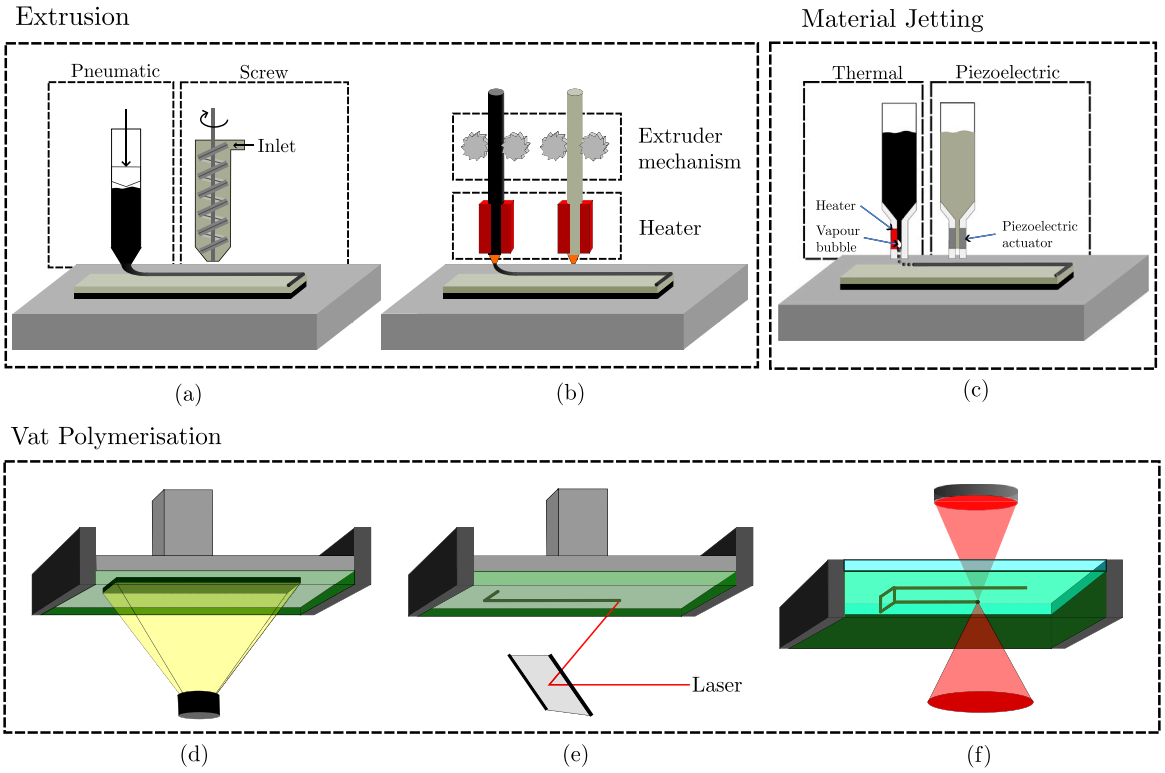

Fig. 3. Portrays a range of 3DP techniques. (a) Direct ink writing (DIW) multi-material setup showcasing both pneumatic and motorised extrusion. (b) Fused deposition modelling (FDM) multi-material configuration using two different thermoplastic filaments. (c) Material jetting (MJ) multi-material configuration with a thermal print mechanism (suited to higher viscosity) and a piezoelectric mechanism (low viscosity). (d) Digital light processing (DLP) projects an entire layer at once to cure the photopolymer. (e) Stereolithography apparatus (SLA) uses a laser to selectively cure a path of the photopolymer. (f) Two photon polymerisation (2PP) where curing only occurs at the focal point of the light projection.

3.1. Single component printing

Single component printing is the most straightforward approach when applying additive manufacturing (AM) techniques in the fabrication of DEA devices, whereby only the dielectric or conductive layers are printed whilst the other component is fabricated via traditional techniques — casting, pre-stretching prefabricated materials, or painting. Since this method only utilises single material printing, an extensive range of AM techniques have been explored. As an example, whilst Vat Polymerisation (VP) is a suitable technique for single component printing, it has not yet been utilised for a fully printed device due to the limitations regarding feedstock material properties and multi-material printing capability. Note that multi-material manufacturing has been achieved [73–75] but not in the context of DEAs.

3.1.1. Fused Deposition Modelling (FDM)

Extrusion based 3DP encompasses versatile and commonly used AM techniques whereby material is extruded continuously through a nozzle. The wide range of available materials and multi-material capability makes these techniques particularly appealing.

From the range of extrusion based techniques, FDM is the most common approach due to the low cost and ease of use. However, whilst suitable for rapid prototyping, FDM suffers from limitations related to lower printing resolutions – particularly in the z-direction – which can result in distortions or higher surface roughness, see Table 1. Moreover, the choice of feedstock is constrained to thermoplastics which typically do not align to the sought after mechanical and electrical properties of the dielectric and conductive layers. On the other hand, multi-material setups – demonstrated in Fig. 3b – are common and accessible.

Thermoplastic polyurethane (TPU) and thermoplastic elastomer (TPE) are the only DEA suitable elastomeric materials able to be printed via FDM. In comparison to standard silicones and acrylics, TPUs and TPEs have higher shore hardness restricting their material compliance [76]. Additionally, thermoplastics are highly susceptible to temperature excluding them from operating in higher temperature environments (i.e. over 50 °C) [76]. Gonzalez et al. [77] developed an FDM printed dielectric layer for a DEA using a commercial TPU filament. Printed with a thickness of 200 μm, it underwent dielectric breakdown at 41 kV/mm, which is comparable to and even outperforming other 3D printed DEA devices. However, the recorded actuation strain was relatively low for the voltage required (see Table 2) [77]. Considering now the compliant electrode layers, conductive, flexible FDM filaments are commercially available [78], although they once again exhibit higher shore hardness and lower conductivity making them less ideal candidate materials.

Zhou et al. [79] demonstrates the possibility to use FDM printing to act as a frame for a DEA gripper, the paper highlights the potential for AM to integrate individual actuators into a complex device without adhesive [79]. The frame alters the actuation characteristics while the DEA materials do not need to be optimised for a printing process, therefore with no detrimental effect to the electro-mechanical properties.

3.1.2. Vat Polymerisation (VP)

VP techniques exploit light sources to cure selected regions or paths on a build plate submerged in a photopolymer resin, enabling layer-by-layer construction to yield a 3D geometry. This method of printing exhibits high resolution in comparison to extrusion based techniques – see Table 1 – which is essential for fabricating optimised geometries with low thickness, critical for reducing the DEA driving voltage. However, whilst the resolution is improved, the typical material properties are still not desirable for both elements of DEA devices and without multi-material printing options, this method lacks critical capability. VP consists of three specific techniques, namely, Stereolithography Apparatus (SLA), Digital Light Processing (DLP) and Two Photon Polymerisation (2PP).

SLA uses a UV laser to selectively cure a liquid photopolymer path (see Fig. 3e), allowing for precise control over the printed part geometry — potentially critical in the miniaturisation of DEA devices for advanced robotics and medical implants. Similar to SLA, DLP utilises UV curable resins, however, the UV light source projects the whole slice, thus curing an entire layer at once (see Fig. 3d). While this improves printing speeds, the light source is pixelated which can result in a non-smooth printed part. This effect can be reduced via anti-aliasing and the enhanced printing speeds can improve the scalability of production.

It can be seen that VP 3DP methods are typically confined to single material printing and thus there is a need to devise alternative approaches to device design. Huang et al. [80] explores a method in which the dielectric layers of a stacked device are printed as a single piece utilising a channel approach. Post printing, the hollow channels can be filled with a conductive material such as carbon grease — see Fig. 4b. Although this device is not all printed, it has significantly streamlined the manufacturing process and demonstrates innovative approaches utilising 3DP for fabricating complex structures.

3.1.3. Material Jetting (MJ)

Material Jetting (MJ), commonly referred to as Inkjetting, uses an ink-based material feedstock which is then jetted as droplets onto a substrate. This process allows for precise control over deposition rates, facilitating the fabrication of thin, uniform layers. The ability to deposit multiple materials in a single process is particularly important in the fabrication of DEA devices [71]. Two methods to create the droplets – thermal and piezoelectric – are shown in Fig. 3c.

Significant research has been undertaken in the multi-material capabilities of MJ and as presented in the upcoming fully printed section, this technology has been used to fully 3D print DEAs. However, a large proportion of current literature has focused on single component printing, particularly soft, flexible conductors.

Traditional MJ setups have been designed around low viscosity inks, which are not suitable for high viscosity silicone feedstock, typically desirable for DEAs. To make these high viscosity silicones suitable, additional preprocessing steps can be conducted to improve the printability such as diluting the ink with a solvent — which consequently can be detrimental to the material properties and increase the cure time significantly. High viscosity jetting is an emerging technique employing specialised printheads and heating systems to accurately deposit more viscous inks, allowing ink formulation to prioritise material properties over printability.

A new technique of MJ which promises higher resolutions is electrohydrodynamic (EHD) jetting. In applying an electric field between the nozzle and the print bed, the ink droplets become charged resulting in attraction to the substrate [81]. The benefits – as described by Liashenko et al. [81] – include printing speeds up to 0.5 mm/s at a submicron scale due to the addition of amplifiers to electrostatically deflect the jet trajectory. Additionally, as a result of the electrostatic forces creating a jet of ink, the nozzle size can be significantly larger than the jet size, thus reducing the risk of clogging. Recently, the use of EHD jetting has been demonstrated by Jiang et al. [82] to print dielectric layers.

3.2. Fully 3D printed DEA devices

Fully printed DEAs describe the printing of both dielectric and conductive DEA components without the need for post-printing assembly. This method of manufacturing ensures the ability to construct sophisticated devices as well as offers significant benefits in both time and performance.

3.2.1. Direct Ink Writing (DIW)

DIW, an extrusion based process, is particularly appealing for the fabrication of DEAs because of its versatility, namely the ability to print a large range of materials including soft elastomers and conductive inks with various curing mechanisms. A disadvantage of this technique is that it has a comparatively lower resolution — see Table 1. There are two main methods of extrusion for DIW as presented in Fig. 3a. The first is pneumatic whereby compressed air ensures a continuous material feed, whereas the second is motorised direct drive, whereby a screw mechanism feeds material through. The latter technique provides increased control since it is either on or off whereas pneumatics can be impacted by residual pressure. However, it is a more complicated system which introduces additional maintenance demands. In the context of multi-material printing, DIW can be split into two categories, specifically, multi-nozzle and single-nozzle systems — both of which are described below.

Multi-Nozzle Printing

Multi-nozzle printing incorporates an array of printing cartridges and nozzles that the system will physically switch between when printing. A paper by Uzel et al. [88] presents the advancement of this technology, not only demonstrating multi-material and multi-nozzle extrusion, but also the ability to print on substrates with arbitrary topography — achieved by first scanning the substrate to calculate the print path. The printing system is fitted with a 16 nozzle array consisting of individual spring loaded nozzles connected to stepper motors via a pulley system, enabling the control of individual nozzle heights while retaining a compact configuration [88]. The ability to print on non-uniform substrates would significantly benefit DEA designs with complex 3D geometries since printing at multiple ‘z’ heights without the need for additional layers provides two key benefits, firstly, smaller thickness which is critical in lowering actuation voltage and secondly, lower risk of delamination which is critical in maintaining maximum elongation and durability of the device.

The vast majority of fully printed DEA devices have used a form of multi-nozzle DIW printing as presented in the non-exhaustive Table 2. Thetpraphi et al. [4] developed a fully printed actuator for optical mirror applications, where the ability to print directly onto an optical mirror surface was demonstrated [4]. Danner et al. [86] presented a fully printed stacked actuator which enabled significantly lower actuation voltages of 3.5 kV for a 75 μm displacement [86]. Note that Table 2 presents details for un-stacked configurations unless stated otherwise.

Multi-Material Single-Nozzle Printing

Multi-material printing does not necessarily have to consist of a multi-nozzle configuration, as portrayed by Chortos et al. [24] where “core-sheath-shell dielectric elastomer fibres DEF” [24] were fabricated (see Fig. 4e). Utilising DIW printing, this paper demonstrates extrusion of a continuous DEA with a dielectric elastomer sandwiched between a

Table 2
Presents the formulation and actuation details of 3DP DEA devices.

Ref.	Ink formulations					Printing method	Actuation details			
	Layer	Base material	Additive 1	Additive 2	Additive 3		Dielectric thickness	Actuation voltage	Actuation strain	Breakdown field strength
[6]	Dielectric Conductive	Ecoflex 00–30 Ecoflex 00–30	SloJo cure retarder SloJo cure retarder	THI-VEX Silicone thinner	– Carbon black	DIW	366 μm	18 kV/mm	8.45%	19.3 kV/mm
[83]	Dielectric Conductive	PUA oligomer PEG-PES	BDDA crosslinker Dithol chain extenders	DOP plasticiser Trithiol crosslinkers	– Carbon black	DIW	380 μm	26 kV/mm	9%	26 kV/mm
[24]	Dielectric Conductive	Ecoflex 00–30 Ecoflex 00–30	CAB-O-SIL TS-720 Carbon black	SloJo cure retarder SloJo cure retarder	SE1700 –	DIW	204 μm	60 kV/mm	10%	60 kV/mm
[85]	Dielectric Conductive	CN9018 CN9028	CAB-O-SIL TS-720 Dioctyl phthalate	Igracure 651 Carbon black	– –	DIW	–	10 kV[a]	–4.4%	14.2–23 kV/mm[a]
[4]	Dielectric Electrode	Terpolymer Terpolymer	Methyl ethyl ketone Carbon black	– –	– –	DIW	100 μm	45 kV/mm	1.025%	87 kV/mm [5]
[86]	Dielectric Electrode	PDMS DBTL PDMS	Hydrophobic silica Carbon black	Methyl-Hydrosiloxane copolymer Methyl-Hydrosiloxane copolymer	Polar polysiloxane DBTL	DIW	210 μm	21 kV/mm	5%	21.93 kV/mm
[26]	Dielectric Electrode	Sylgard 184 JS-A211	Octyl acetate (40% Ag nanoparticle)	– –	– –	Inkjetting	–	1 kV_{pp}	36 μm	–
[87]	Dielectric Electrode	NinjaFlex TPU Eel TPU 3D	– –	– –	– –	FDM	150 μm	25 kV/mm	–	38 kV/mm
[84]	Dielectric Conductive	PDMS Silver paint	TRGO400 –	– –	– –	Inkjetting Screen printing	430 μm	5 kV/mm	6.7%	7 kV/mm
[77]	Dielectric Electrode	Diabase X60 ultra flexible TPU Carbon grease	– –	– –	– –	FDM n/a	200 μm	41 kV/mm	4.91–5.71%*	41 kV/mm
[80]	Dielectric Electrode	Ebecryl 8413 Carbon grease	Ebecryl 113 –	– –	– –	DLP n/a	500 μm	13 kV/mm	55 μm	40.9 kV/mm

[a] Due to the design of the HDEA there is no constant distance between the electrodes and therefore the breakdown voltage is provided via calculation [85]. Fully printed methods are colour coded whilst single component printed methods are coloured grey within the method column.

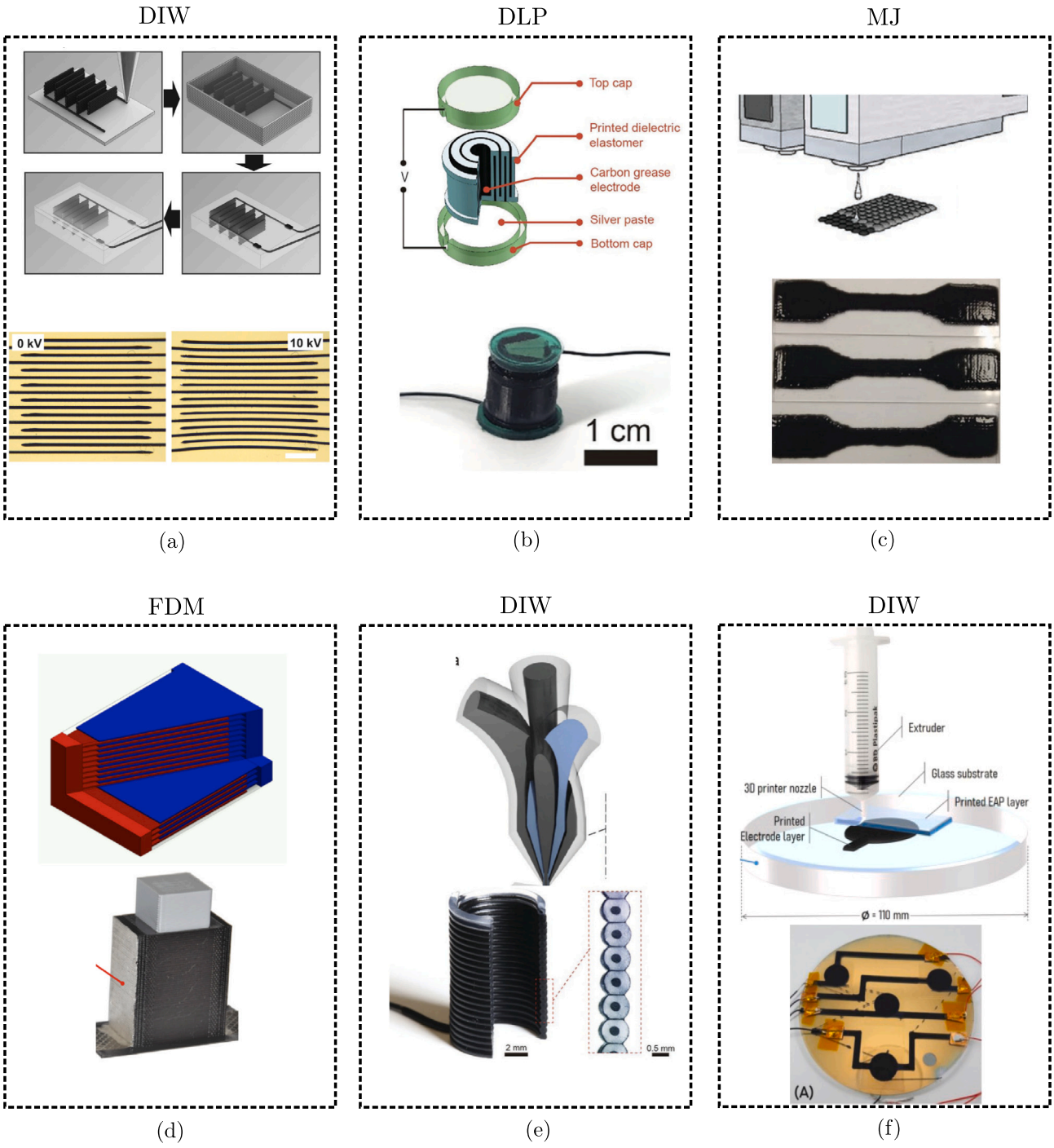

Fig. 4. Displays single component 3D printed devices in a–c ((a) DIW printed electrodes reproduced from [83]. (b) DLP printed dielectric device reproduced from [80]. (c) MJ printed enhanced dielectric layer reproduced from [84]) and fully 3D printed DEA devices d–f ((d) FDM printed stacked actuator reproduced from [25]. (e) DIW printed dielectric elastomer fibre (DEF) reproduced from [24]. (f) DIW printed EAP for optical mirror applications reproduced from [4].

conductive core and shell. The fibre design is significantly different to the traditional planar DEAs and previously was only possible through a complex manufacturing process whereby an elastomer was manually coated with both electrode and dielectric layers [89]. The technique used in this paper is capable of simultaneously printing all layers – or just selected layers – through a single divided nozzle, enabling the fibres to be printed with complex 3D geometries including passive regions (where the outer electrode is not printed) thus yielding stretching, bending and steerable bundles. Zhu et al. [90] also utilises this technique to develop an insect scale soft robot, using a coiled DEF to act as an artificial muscle integrated with rigid DLP printed robotic components [90].

Further extending the single-nozzle technique, Larson et al. [85] showcases the ability to print "helical dielectric elastomer actuators HDEA"[85] (see Fig. 4f) by developing a system which combines both multi-material and rotational 3D printing of a single filament. The printer extrudes filament using a continuously rotating multi-material nozzle with programmable helix angle, layer thickness and interfacial area between the materials within the nozzle [85]. HDEAs enable sophisticated actuations whereby an applied electric field results in an torsional actuation leading to an axial strain.

3.2.2. FDM

Through a multi-nozzle FDM approach, Raguž et al. [87] developed a dielectric elastomer gripper. This fabrication technique enabled the production of an anisotropic actuator where the anisotropy was introduced through the infill direction. When activated with 4.5 kV, a 16 mm difference in strain was observed between the sample printed in vertical and horizontal directions [87]. The benefits of a fully FDM printed device is the durability and potential for optimisation of electrode placement whilst also simplifying the manufacturing process in comparison to single component printing.

An additional example of fully printed DEA device via FDM is presented by Palmić et al. [25], where a stacked configuration with up to 100 DE layers was fabricated. Stacking is advantageous in reducing the operating voltage and the use of commercially available thermoplastic filaments shows the potential for scalability. However, to achieve these results, optimising the reliability and repeatability were essential as a defect in one layer can compromise the whole device.

3.2.3. MJ

MJ is another AM technique with significant interest in DEA manufacture. Malas et al. [84] developed PDMS based dielectric inks with graphene, graphene oxide, and thermally reduced graphene oxide fillers. The addition of 1.5% weight of thermally reduced graphene oxide resulted in an increase in displacement from 0.3–6.7% compared to pure PDMS, however, the dielectric breakdown strength was significantly reduced from 26 kV/mm to 7 kV/mm [84]. The breakdown limitation may be caused by the jetting mechanism, where variations in filler distribution within the deposited film can occur due to filler agglomeration triggering electric breakdown as it approaches the percolation threshold [84]. Yi et al. [91] has also shown the potential to develop electrodes for DEAs using inkjetting, obtaining a resolution of 25 μm for single line printing [91].

Fully-printed DEA devices are still uncommon with this technique, although, Gallucci et al. [26] has established a method for printing both electrodes and elastomers using this technique. The electrodes were fabricated using a silver nanoparticle ink while the dielectric was made from Sylgard 184 (DOW) diluted in a solvent [26]. However this process required significant processing between layers to enable curing and enhance adhesion.

4. Challenges to fully print DEA devices

The development of fully 3DP DEAs represents a significant advancement in soft robotics, haptics, and other emerging applications where flexibility, lightweight design, and high-performance actuation are paramount. Over the past five years, extensive progress has been made in integrating 3DP techniques with DEA fabrication, providing new opportunities for complex, multi-functional designs. However, despite these advancements, critical challenges continue to restrict the realisation of fully 3D-printed DEAs that can satisfy the mechanical, electrical, and actuation demands of real-world applications. The challenges associated with fully 3DP DEA devices can be split into three main areas: material-related, process-related, and actuation-related. These are shown in Fig. 5, providing a visual representation of the design, manufacture and actuation variables and the reliance on material formulation to maximise the final properties of the device.

4.1. Material-related challenges

The formulation of the conductive and dielectric materials must be optimised in such a way that a balance is found between a DEAs electrical and mechanical properties. However, when manufacturing these actuators using 3DP techniques, such as DIW, the uncured feedstocks rheological properties must be considered to ensure printability. These inks must exhibit shear thinning behaviour, whereby the viscosity decreases under applied shear stress, ensuring the ink flows consistently through the nozzle during printing, while recovering and maintaining structure after deposition. Therefore, material formulation must balance the printability with the electro-mechanical properties, essential for effective actuation performance. During material formulation, additives are often used to enhance the printability as well as the dielectric or conductive properties, but this often becomes detrimental for the mechanical performance and durability.

4.1.1. Dielectric ink formulation

Dielectric elastomer inks must have the required mechanical and dielectric characteristics for actuation. These inks are typically based on soft elastomer materials such as silicones — which typically will not possess the rheological properties necessary to print, especially as the nozzle size decreases.

One approach used to produce shear thinning behaviour in dielectric inks is to embed dielectric nano-particles as explored by Lyu et al. [92] by analysing composites with a polydimethylsiloxane (PDMS) matrix and carbon, metallic, or ceramic fillers. The results of the study indicated that while PDMS alone behaves as a Newtonian fluid, as carbon is added in increasing amounts the composite ink displays shear thinning characteristics with increasing storage modulus and viscosity (at low shear rates) [92].

Alternatively, to increase shear thinning characteristics in silicones, commercial thixotropic additives can be incorporated such as THIVEX (Smooth On). A key advantage to this technique is that using a liquid additive removes the possibility of dielectric breakdown occurring due to concentrations of filler particles. The effect of breakdown due to particle concentrations could be a result of space charge [93] whereby excess electric charge acts as a continuum, with the effect more prominent when particles are unevenly distributed.

Optimising material formulations for printability often results in detrimental impacts for the electro-mechanical properties of the cured material. Danner et al. [86] developed a material formulation in which tuning the ink printability can be uncoupled from the electro-mechanical properties of interest, using the principles of capillary suspensions [86]. This is achieved by incorporating a small secondary immiscible liquid phase into the polysiloxane matrix forming a capillary bridge between the solid filler particles. The rheological properties are changed by altering the concentration and properties of the secondary fluid, while the bulk material properties remain unaffected due to secondary fluids confinement to the filler interface [86]. Mehnert et al. [94] also investigated the electro-mechanical response of elastomers filled with high dielectric permittivity particles and found that although the particles contributed to the stiffening of the material they enhanced the effect of the electric field. Additionally a study by Kumar et al. [95] found that when curing silicones with dielectric particles under an electric field, the material had improved dielectric and mechanical properties, whilst also reducing particle agglomeration.

4.1.2. Conductive ink formulation

The formulation of conductive inks is equally important for the creation of compliant electrodes in DEAs. These inks must be electrically conductive, highly deformable, and capable of forming thin, uniform layers that maintain conductivity even under large strains.

A common approach to fabricating these conductive layers is to embed conductive nano-particles in silicones. This method yields the desired electrical and mechanical properties, as well as ensuring the shear thinning characteristics [92]. Furthermore, in using a similar silicone matrix, compatibility between the conductive and dielectric layers is improved. However, the addition of solid particles into elastomers can present significant challenges whereby concentrations can change the local mechanical properties increasing the risk of tearing and delamination. Therefore, it is essential to take steps to ensure proper dispersion of filler particles leading to the homogenisation of the ink formulation. For example, Chortos et al. [24] mixed their conductive ink formulation for a total of 32 min using a bladeless

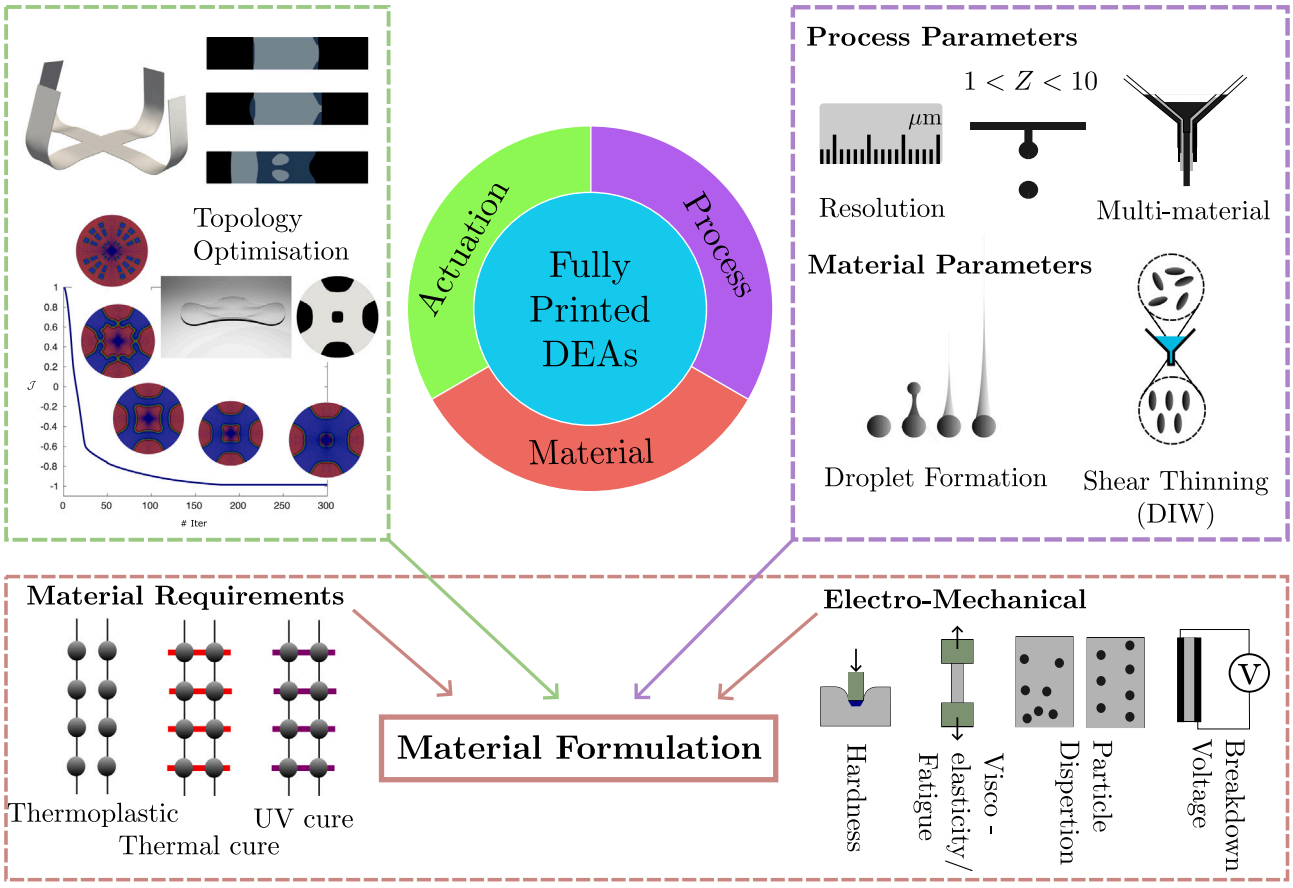

Fig. 5. Presents the challenges associated with fully printed DEA devices broken into three distinct categories relating to the print process, the material formulations, and the device actuations.

centrifugal mixer and roll milled three times. Upon homogenisation of the ink, it was placed into a centrifuge to remove trapped air [24]. Common filler particles of choice are carbon black due to its high conductivity and relative low cost, as well as silver, copper and other conductive particles [26,92].

4.2. Process-related challenges

Whilst AM is still in its infancy, it is rapidly developing — take for example DIW in which considerable research has taken place over the past five years. Wu et al. [96] has highlighted the difficulty of printing high viscosity pastes containing micron-sized particles in the micro-scale. Multiple studies have successfully improved printability via a combination of experimental study, machine learning and simulation to optimise material flow [97–99]. However, this paper focuses on the type of nozzle used. In this paper it was found that using glass nozzles resulted in a 100× increase in printing speed due to glass exhibiting the wall slip effect [96]. Additionally, the lack of friction prevents particle agglomeration, a cause of clogging and inconsistent flow [96]. As highlighted above, embedding particles is essential in developing printable compliant electrodes and improvements in this area will continue to increase the feasibility of smaller soft robotics and reduced actuation voltage. However, as with all other challenges, effective printing relies on material formulation and the rheological properties.

4.3. Actuation-related challenges

3DP has enabled the fabrication of complex DEA designs, however, the actuation performance of these devices is still limited by several factors. Conventionally manufactured DEA devices have demonstrated high area strains of over 189% [100,101], far higher than those achieved by fully 3D printed devices (see Table 2). As there is no need to optimise material properties relating to a specific printing process, conventionally manufactured DEA devices can be optimised for the best electro-mechanical performance. Shi et al. [100] demonstrates a material formulation with a breakdown voltage of 330 kV/mm, an order of magnitude higher than most printable compositions presented in Table 2, which could be due to voids/imperfections in printed layers, as well as material formulation constraints. Moreover, Feng et al. [101] has presented a DEA device that can achieve an area strain of 254% at a driving voltage of only 46 kV/mm. However, the actuation of these devices is limited to simple bending or expansion compared to the complex actuations achievable with additive manufacturing.

Although not the focus of this review, DEA devices continue to be limited by a number of factors, primarily their high voltage requirement (see Table 2). To provide a high output voltage, most researchers rely on high voltage amplifiers (typically large and heavy) which result in the tethering of the DEA device thereby limiting their applications. Whilst the high voltage requirement can be alleviated by improving electro-mechanical responsiveness through material formulation or device geometry, such as the 300 V, 3 μm actuator by Poulin et al. [102], research is also being conducted on the miniaturisation of high voltage DC–DC voltage multipliers [103] providing another potential solution to eventually untether these actuator devices. These advancements are likely to drive research in DEA devices as feasibility for the fabrication of small, soft, untethered robotics increases.

5. Summary and outlook

3DP clearly demonstrates the capacity to pave the way in the fabrication of DEA devices, specifically enabling the creation of complex,

multi-material structures with enhanced performance and functionality. Nevertheless, critical challenges remain with regards to material compatibility, geometric complexity, printing resolution, and scalability. Overcoming these challenges requires continued research and development in both material science and 3DP technologies, and will ultimately revolutionise soft robotics for use in a vast range of fields.

5.1. Advancements in 3D printing technology

Section 4 has highlighted a range of challenges associated with 3DP, but it is important to note that all forms of 3DP are improving thanks to academic and industrial research. For example, the most common and cost effective 3DP method, FDM, has seen vast improvements in quality and print speed due to companies such as Bambu Labs [104] and Creality [105]. Furthermore, they have developed systems for multi-colour printing whereby materials with similar profiles can be deposited through a single nozzle.

Other companies such as SYGNIS, a company focused on DIW technology, have been exploring 3DP soft robotics — developing a DP silicone gripper [106]. CellInk, a company dedicated to bioprinting, have also developed DIW technology with the BIO X6 capable of printing with six printheads in one process as well as the BIONOVA X 3D high resolution, multi-material DLP printer, capable of tuning the stiffness gradients in the printed material [107].

Improvements to MJ techniques are also being made by companies such as Inkbit. For example they have developed "Vision-Controlled Jetting (VCJ)" which uses a 3D scanner to provide feedback during the printing process, eliminating defects from the previous layer [108]. Buchner et al. [109] uses this technology to develop a high resolution, tendon driven hand, made up of both soft and hard components [109].

Different methods of 3DP have specific capabilities which may align better for fabricating certain components — for example VP methods have a limited ability to print conductive particle embedded feedstocks due to the particles blocking the light source. To handle this dilemma multi-method printers have been developed which can exploit multiple 3DP methods in a single manufacturing process. Table 3 displays some prominent printers and their associated features from both industrial and research backgrounds. Roach et al. [110] developed the "m^4 3D printer" [110] integrating FDM, DIW, MJ and aerosol jetting with UV curing and a robotic arm. This printer enables dissimilar materials to be incorporated into a fully printed DEA without the material restrictions imposed by a single-method printer. Furthermore, this combination of printing methods is advancing commercially with companies such as RegenHu offering printers with five dispensing slots for six different dispensing methods [111], or Desktop Metal's 3D-Bioplotter with modular tool changer compatible with extrusion and jetting print heads capable of 500 °C heating and UV curing [112]. Multi-method printing is not only limited to extrusion and jetting, Whitehead et al. [113] presents a printer combining SLA and SLS technology (Selective laser sintering — powder is fused together to generate a structure) [113]. TPU in powder form, could enable SLS to fabricate elastomeric materials for DEA devices, however, a considerable disadvantage to this method is the resulting high porosity of the material. The addition of SLA improves the surface finish and widens the available materials whilst also reducing the porosity of the SLS printed component. Since this technique is in early stages of development, there are still issues such as material cross contamination — critical when considering conductive and dielectric materials in the same print process.

Exploring vat based multi-method printing, Peng et al. [114] developed a printer containing both DLP and DIW methods [114]. This enabled both the printing of elastomer resins and electronic inks, highlighting the possibility for this process to be adopted for the fabrication of a DEA device. This approach circumvents one of the challenges associated withDLP printing conductive materials, where embedded particles block UV light inhibiting uniform curing.

5.2. Conclusion

The integration of 3DP in the fabrication of DEAs represents significant potential in the growth of research in the fields of soft robotics, biomimetics, and adaptive systems to name a few. This mini-review has explored the progress made in 3DP technologies towards the realisation of fully printed DEA devices, emphasising the association between computational design and physical manufacturing. By leveraging 3DP, researchers have been able to fabricate increasingly complex and highly optimised actuator designs that were previously unachievable using traditional methods such as casting or manual assembly. The ability to directly print intricate geometries, multi-material structures, and miniaturised components has unlocked new possibilities for DEAs, extending their potential applications across various fields, including artificial muscles, wearable haptics, soft robotics, and bio-integrated systems.

However, despite these advancements, several critical challenges remain that hinder the widespread adoption of fully 3DP DEAs. Material formulation remains one of the most significant obstacles, as it requires a delicate balance between mechanical properties, dielectric strength, conductivity, and printability. Whilst conductive inks and dielectric elastomers have been developed for specific printing techniques such as DIW, FDM, and MJ, the compromise between electrical and mechanical performance must be carefully managed. Many of the currently available printable materials still fall short of the properties exhibited by conventionally processed DEAs, particularly in terms of dielectric breakdown strength and long-term mechanical stability.

Another major challenge lies in multi-material integration and printing resolution. The ability to precisely deposit multiple functional materials within a single manufacturing process is crucial for achieving fully printed DEAs, as it ensures proper layering of dielectric and conductive components without requiring post-processing or manual assembly. Whilst some progress has been made in developing single and multi-nozzle printing techniques, as well as hybrid manufacturing systems that combine different 3DP methods (see Table 3), these approaches often introduce new complexities, such as weak interfacial adhesion, material compatibility concerns, and increased processing time. Additionally, resolution constraints in extrusion-based methods compared to MJ and VP technologies can lead to surface roughness and inhomogeneous material distribution, which may impact the actuator's performance, durability, and reliability.

Furthermore, actuation performance and scalability remain prominent limitations in the development of fully printed DEAs. The high voltage requirements for actuation, typically ranging from 1 to 10 kV, pose significant challenges for real-world applications, particularly in mobile and untethered soft robotic systems. Reducing the operating voltages whilst maintaining high strain output, requires innovative approaches in both material development (e.g. high-permittivity elastomers, nano-particle dielectrics), and device engineering (e.g. stacked configurations, optimised electrode placement). In addition, whilst 3DP techniques have enabled greater reproducibility and customisation, ensuring scalability and industrial feasibility is still a significant obstacle, as printing times, cost of specialised materials, and consistency of printed devices vary widely across different methods.

Despite these challenges, the future of fully 3DP DEAs is promising. Advances in computational design and topology optimisation continue to enhance the efficiency and functionality of actuator geometries, offering more sophisticated and efficient designs that take full advantage of AM capabilities. The development of next-generation multi-method printing systems, capable of seamlessly integrating soft elastomers, conductive inks, and functionalised nanocomposites, will be essential in pushing the boundaries of DEA performance. Moreover, progress in miniaturised high-voltage electronics and energy-efficient actuation mechanisms will further support the transition towards fully autonomous and mobile soft robotic systems.

Table 3
Displays an overview of a range of multi-method 3D printers.

Company/Research group	Printing types	Additional features	Materials
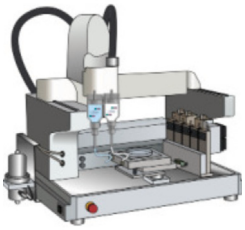 3D-Bioplotter (Desktop metal) (Image from [115])	• Low temperature (DIW) • Ultra-high temperature (DIW/FDM) • Inkjet • 2 component (DIW) • Co-axial • Photo curing	• PrintRoll (3D printing on rotating cylinder) • Printhead cleaning • Modular printheads • Particle filter	• PCL • Hydroxyapatite • Silicones • Biomaterials
 R-GEN 100 (RegenHu [111])	• Inkjet • DIW • FDM • Electro-writing/spinning	• Photocuring • Substraight height calibration • Needle length calibration • Printhead thermal management	• Biomaterials • Conductive inks • Thermoplastics • Elastomers • Pastes • Adhesives
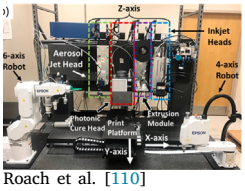 Roach et al. [110]	• Inkjet • FFF (FDM) • DIW • Aerosol jetting	• Pick and place • UV curing • Photonic curing (pulsed light sintering)	• Elastomer resin • Conductive ink • Thermoplastics • Ceramics • Adhesives
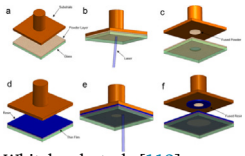 Whitehead et al. [113]	• SLA • SLS	• Reduces porosity of powder fusion part	• Powdered TPU • Resin
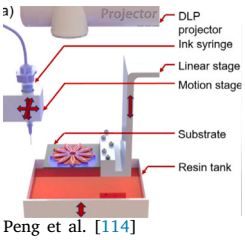 Peng et al. [114]	• DIW • DLP	• Layer thickness compensation • Electronics printing	• Elastomer resin • Commercial resin • Photocurable ink • Liquid crystal elastomer ink • Conductive silver ink

In conclusion, the successful integration of AM into DEA fabrication has the potential to revolutionise a wide range of industries, from healthcare and biomedical devices to soft robotics and haptic technologies. As research continues to address current limitations, fully printed DEAs will become increasingly viable for commercial and industrial applications, ultimately unlocking new possibilities for next-generation soft actuators with unprecedented levels of complexity, functionality, and efficiency.

CRediT authorship contribution statement

Rollo Pattinson: Writing – review & editing, Writing – original draft, Methodology, Formal analysis, Data curation, Conceptualization. **Nathan Ellmer:** Writing – review & editing, Writing – original draft, Investigation, Data curation, Conceptualization. **Mokarram Hossain:** Writing – review & editing, Visualization, Validation, Supervision, Methodology, Funding acquisition, Formal analysis. **Rogelio Ortigosa:** Writing – review & editing, Visualization, Validation, Formal analysis, Data curation. **Jesús Martínez-Frutos:** Writing – review & editing, Visualization, Validation, Formal analysis, Data curation. **Antonio J. Gil:** Writing – review & editing, Visualization, Validation, Supervision, Resources, Project administration, Methodology, Funding acquisition, Formal analysis, Conceptualization. **Anil Bastola:** Writing – review & editing, Writing – original draft, Visualization, Validation, Supervision, Resources, Methodology, Formal analysis, Data curation, Conceptualization.

Declaration of competing interest

The authors declare that they have no known competing financial interests or personal relationships that could have appeared to influence the work reported in this paper.

Acknowledgements

The authors wish to acknowledge the support provided by the Defence, Science and Technology Laboratory (Dstl). A.J. Gil also wishes to acknowledge The Leverhulme Trust Foundation (UK) through a Leverhulme Fellowship. R. Ortigosa and J. Martínez-Frutos acknowledge funding received from grant PID2022-141957OA-C22 funded by MICIU/AEI /10.13039/501100011033/ and by "ERDF A way of making Europe". R. Ortigosa also acknowledges the support provided by the Autonomous Community of the Region of Murcia, Spain, through the programme for the development of scientific and technical research by competitive groups (21996/PI/22), included in the Regional Program for the Promotion of Scientific and Technical Research of Fundación Séneca - Agencia de Ciencia *y* Tecnología de la Región de Murcia. M. Hossain acknowledges the support of the EPSRC via a Standard Grant (EP/Z535710/1) and the Royal Society (UK) through the International Exchange Grant (IEC/NSFC/211316).

Data availability

Data will be made available on request.

References

[1] N. El-Atab, R.B. Mishra, F. Al-Modaf, L. Joharji, A.A. Alsharif, H. Alamoudi, M. Diaz, N. Qaiser, M.M. Hussain, Soft actuators for soft robotic applications: A review, Adv. Intell. Syst. (ISSN: 2640-4567) 2 (10) (2020) http://dx.doi.org/10.1002/aisy.202000128.

[2] Y. Guo, L. Liu, Y. Liu, J. Leng, Review of dielectric elastomer actuators and their applications in soft robots, Adv. Intell. Syst. 3 (10) (2021) 2000282, http://dx.doi.org/10.1002/aisy.202000282, URL https://onlinelibrary.wiley.com/doi/abs/10.1002/aisy.202000282.

[3] A. Bruschi, D.M. Donati, P. Choong, E. Lucarelli, G. Wallace, Dielectric elastomer actuators, neuromuscular interfaces, and foreign body response in artificial neuromuscular prostheses: A review of the literature for an in vivo application, Adv. Heal. Mater. 10 (13) (2021) 2100041, http://dx.doi.org/10.1002/adhm.202100041, URL https://onlinelibrary.wiley.com/doi/abs/10.1002/adhm.202100041.

[4] K. Thetpraphi, W. Kanlayakan, S. Chaipo, G. Moretto, J. Kuhn, D. Audigier, M.Q. Le, P.J. Cottinet, L. Petit, J.F. Capsal, 3D-printed electroactive polymer force-actuator for large and high precise optical mirror applications, Addit. Manuf. (ISSN: 22148604) 47 (March) (2021) 102199, http://dx.doi.org/10.1016/j.addma.2021.102199.

[5] K. Thetpraphi, S. Chaipo, W. Kanlayakan, P.J. Cottinet, M.Q. Le, L. Petit, D. Audigier, J. Kuhn, G. Moretto, J.F. Capsal, Advanced plasticized electroactive polymers actuators for active optical applications: Live mirror, Adv. Eng. Mater. (ISSN: 15272648) 22 (2020) http://dx.doi.org/10.1002/adem.201901540.

[6] E. Zhang, T. Pang, Y. Zhang, F. Huang, M. Gong, X. Lin, D. Wang, L. Zhang, Fully 3D printed dielectric elastomer actuators based on silicone and its composites, Polym. Compos. (ISSN: 15480569) (December 2023) (2024) 1–13, http://dx.doi.org/10.1002/pc.28626.

[7] E. Hajiesmaili, D.R. Clarke, Dielectric elastomer actuators, J. Appl. Phys. (ISSN: 0021-8979) 129 (15) (2021) 151102, http://dx.doi.org/10.1063/5.0043959.

[8] M. Artusi, M. Potz, J. Aristiźabal, C. Menon, S. Cocuzza, S. Debei, Electroactive elastomeric actuators for the implementation of a deformable spherical rover, IEEE/ASME Trans. Mechatronics (ISSN: 10834435) 16 (2011) 50–57, http://dx.doi.org/10.1109/TMECH.2010.2090163.

[9] C.T. Nguyen, H. Phung, T.D. Nguyen, H. Jung, H.R. Choi, Multiple-degrees-of-freedom dielectric elastomer actuators for soft printable hexapod robot, Sensors Actuators A: Phys. (ISSN: 09244247) 267 (2017) 505–516, http://dx.doi.org/10.1016/j.sna.2017.10.010.

[10] G.K. Lau, H.T. Lim, J.Y. Teo, Y.W. Chin, Lightweight mechanical amplifiers for rolled dielectric elastomer actuators and their integration with bio-inspired wing flappers, Smart Mater. Struct. (ISSN: 09641726) 23 (2014) http://dx.doi.org/10.1088/0964-1726/23/2/025021.

[11] G.K. Lau, S.C.K. Goh, L.L. Shiau, Dielectric elastomer unimorph using flexible electrodes of electrolessly deposited (ELD) silver, Sensors Actuators A: Phys. (ISSN: 09244247) 169 (2011) 234–241, http://dx.doi.org/10.1016/j.sna.2011.04.037.

[12] H. Imamura, K. Kadooka, M. Taya, A variable stiffness dielectric elastomer actuator based on electrostatic chucking, Soft Matter (ISSN: 17446848) 13 (2017) 3440–3448, http://dx.doi.org/10.1039/c7sm00546f.

[13] A. Moss, M. Krieg, K. Mohseni, Modeling and characterizing a fiber-reinforced dielectric elastomer tension actuator, IEEE Robot. Autom. Lett. (ISSN: 23773766) 6 (2021) 1264–1271, http://dx.doi.org/10.1109/LRA.2021.3056349.

[14] M. Duduta, D.R. Clarke, R.J. Wood, A high speed soft robot based on dielectric elastomer actuators, in: 2017 IEEE International Conference on Robotics and Automation, ICRA, IEEE, ISBN: 978-1-5090-4633-1, 2017, pp. 4346–4351, http://dx.doi.org/10.1109/ICRA.2017.7989501, URL http://ieeexplore.ieee.org/document/7989501/.

[15] Web of science, 2025, https://www.webofscience.com/wos/woscc/advanced-search. (Accessed 03 January 2025).

[16] C. Keplinger, M. Kaltenbrunner, N. Arnold, S. Bauer, Röntgen's electrode-free elastomer actuators without electromechanical pull-in instability, Proc. Natl. Acad. Sci. USA (ISSN: 00278424) 107 (2010) 4505–4510, http://dx.doi.org/10.1073/pnas.0913461107.

[17] R.H. Gaylord, Fluid actuated motor system and stroking device, 1958, Patent number: 2, 844, 126.

[18] R. Snelson, A. Karchak, V.L. Nickel, Application of external power in upper extremity orthotics*, Orthop. Prosthet. Appl. J. (1961) 345–348.

[19] B. Tondu, Modelling of the McKibben artificial muscle: A review, J. Intell. Mater. Syst. Struct. (ISSN: 1045389X) 23 (2012) 225–253, http://dx.doi.org/10.1177/1045389X11435435.

[20] R. Pelrin, R. Kornbluh, Q. Pei, J. Joseph, High-speed electrically actuated elastomers with strain greater than 100, Science 287 (2000) 836–839, http://dx.doi.org/10.1126/science.287.5454.83, URL https://www.science.org/doi/10.1126/science.287.5454.836.

[21] K. Jung, K.J. Kim, H.R. Choi, A self-sensing dielectric elastomer actuator, Sensors Actuators A: Phys. (ISSN: 09244247) 143 (2008) 343–351, http://dx.doi.org/10.1016/j.sna.2007.10.076.

[22] M. Landgraf, S. Reitelshofer, J. Franke, M. Hedges, Aerosol jet printing and lightweight power electronics for dielectric elastomer actuators, in: 2013 3rd International Electric Drives Production Conference, EDPC, IEEE, ISBN: 978-1-4799-1105-9, 2013, pp. 1–7, http://dx.doi.org/10.1109/EDPC.2013.6689733, URL http://ieeexplore.ieee.org/document/6689733/.

[23] S. Hunt, T.G. McKay, I.A. Anderson, A self-healing dielectric elastomer actuator, Appl. Phys. Lett. (ISSN: 00036951) 104 (2014) http://dx.doi.org/10.1063/1.4869294.

[24] A. Chortos, J. Mao, J. Mueller, E. Hajiesmaili, J.A. Lewis, D.R. Clarke, Printing reconfigurable bundles of dielectric elastomer fibers, Adv. Funct. Mater. (ISSN: 16163028) 31 (22) (2021) 1–10, http://dx.doi.org/10.1002/adfm.202010643.

[25] T.B. Palmić, J. Slavič, Single-process 3D-printed stacked dielectric actuator, Int. J. Mech. Sci. (ISSN: 00207403) 230 (2022) http://dx.doi.org/10.1016/j.ijmecsci.2022.107555.

[26] G. Gallucci, Y. Wu, M. Tichem, A. Hunt, Fully inkjet-printed dielectric elastomer actuators, in: J.D.W. Madden, S.S. Seelecke, A.L. Skov (Eds.), Electroactive Polymer Actuators and Devices (EAPAD) XXVI, Vol. 12945, International Society for Optics and Photonics, SPIE, 2024, 129450I, http://dx.doi.org/10.1117/12.3010872.

[27] J.-P. Crine, Influence of electro-mechanical stress on electrical properties of dielectric polymers, IEEE Trans. Dielectr. Electr. Insul. (ISSN: 1070-9878) 12 (2005) 791–800, http://dx.doi.org/10.1109/TDEI.2005.1511104, URL http://ieeexplore.ieee.org/document/1511104/.

[28] R. Pelrine, R. Kornbluh, G. Kofod, High-strain actuator materials based on dielectric elastomers, Adv. Mater. (ISSN: 09359648) 12 (2000) 1223–1225, http://dx.doi.org/10.1002/1521-4095(200008)12:16<1223::AID-ADMA1223>3.0.CO;2-2.

[29] P. Brochu, Q. Pei, Advances in dielectric elastomers for actuators and artificial muscles, 2010, ISSN 10221336.

[30] H. Zhang, H. Wen, J. Zhu, Z. Xia, Z. Zhang, 3D printing dielectric elastomers for advanced functional structures: A mini-review, 2024, ISSN 10974628.

[31] A. Zolfagharian, A.Z. Kouzani, S.Y. Khoo, A.A.A. Moghadam, I. Gibson, A. Kaynak, Evolution of 3D printed soft actuators, Sensors Actuators A: Phys. (ISSN: 09244247) 250 (2016) 258–272, http://dx.doi.org/10.1016/j.sna.2016.09.028.

[32] S.Q. Ma, Y.P. Zhang, M. Wang, Y.H. Liang, L. Ren, L.Q. Ren, Recent progress in 4D printing of stimuli-responsive polymeric materials, Sci. China Technol. Sci. (ISSN: 18691900) 63 (2020) 532–544, http://dx.doi.org/10.1007/s11431-019-1443-1.

[33] X. Wang, M. Jiang, Z. Zhou, J. Gou, D. Hui, 3D printing of polymer matrix composites: A review and prospective, 2017, ISSN 13598368.

[34] X. Ji, X. Liu, V. Cacucciolo, M. Imboden, Y. Civet, A.E. Haitami, S. Cantin, Y. Perriard, H. Shea, An autonomous untethered fast soft robotic insect driven by low-voltage dielectric elastomer actuators, Sci. Robot. 4 (2019) http://dx.doi.org/10.1126/scirobotics.aaz6451, URL https://www.science.org.

[35] Y. Chen, H. Zhao, J. Mao, P. Chirarattananon, E.F. Helbling, N. seung Patrick Hyun, D.R. Clarke, R.J. Wood, Controlled flight of a microrobot powered by soft artificial muscles, Nature (ISSN: 14764687) 575 (2019) 324–329, http://dx.doi.org/10.1038/s41586-019-1737-7.

[36] Y. Tang, L. Qin, X. Li, C.-M. Chew, J. Zhu, A frog-inspired swimming robot based on dielectric elastomer actuators, in: 2017 IEEE/RSJ International Conference on Intelligent Robots and Systems, IROS, IEEE, Vancouver, BC, Canada, ISBN: 978-1-5386-2682-5, 2017, pp. 2403–2408, http://dx.doi.org/10.1109/IROS.2017.8206054, URL http://ieeexplore.ieee.org/document/8206054/.

[37] J. Shintake, H. Shea, D. Floreano, Biomimetic underwater robots based on dielectric elastomer actuators, in: 2016 IEEE/RSJ International Conference on Intelligent Robots and Systems, IROS, IEEE, ISBN: 978-1-5090-3762-9, 2016, pp. 4957–4962, http://dx.doi.org/10.1109/IROS.2016.7759728, URL http://ieeexplore.ieee.org/document/7759728/.

[38] Y. Qiu, E. Zhang, R. Plamthottam, Q. Pei, Dielectric elastomer artificial muscle: Materials innovations and device explorations, Acc. Chem. Res. (ISSN: 15204898) 52 (2019) 316–325, http://dx.doi.org/10.1021/acs.accounts.8b00516.

[39] S. Shian, R.M. Diebold, A. McNamara, D.R. Clarke, Highly compliant transparent electrodes, Appl. Phys. Lett. (ISSN: 00036951) 101 (2012) http://dx.doi.org/10.1063/1.4742889.

[40] S. Shian, R.M. Diebold, D.R. Clarke, Tunable lenses using transparent dielectric elastomer actuators, Opt. Express (ISSN: 10944087) 21 (2013) 8669, http://dx.doi.org/10.1364/oe.21.008669.

[41] A.K. Sharma, M. Kosta, G. Shmuel, O. Amir, Gradient-based topology optimization of soft dielectrics as tunable phononic crystals, Compos. Struct. (ISSN: 02638223) 280 (2022) http://dx.doi.org/10.1016/j.compstruct.2021.114846.

[42] K.X. Huang, G.S. Shui, Y.Z. Wang, Y.S. Wang, Meta-arrest of a fast propagating crack in elastic wave metamaterials with local resonators, Mech. Mater. (ISSN: 01676636) 148 (2020) http://dx.doi.org/10.1016/j.mechmat.2020.103497.

[43] K.X. Huang, G.S. Shui, Y.Z. Wang, Y.S. Wang, Enhanced fracture resistance induced by coupling multiple degrees of freedom in elastic wave metamaterials with local resonators, J. Elasticity (ISSN: 15732681) 144 (2021) 33–53, http://dx.doi.org/10.1007/s10659-021-09825-9.

[44] M. Shrestha, G.K. Lau, Y.W. Chin, E.H. Teo, B.C. Khoo, Z.B. Lu, A tunable acoustic absorber using reconfigurable dielectric elastomer actuated petals, Commun. Eng. (ISSN: 27313395) 3 (2024) http://dx.doi.org/10.1038/s44172-023-00159-z.

[45] M. Shrestha, L. Depari, E.H. Teo, Printable transparent conductive ink for dielectric elastomer-based tunable acoustic absorber, in: FLEPS 2024 - IEEE International Conference on Flexible and Printable Sensors and Systems, Proceedings, Institute of Electrical and Electronics Engineers Inc., ISBN: 9798350383263, 2024, http://dx.doi.org/10.1109/FLEPS61194.2024.10604244.

[46] X. Qu, X. Ma, B. Shi, H. Li, L. Zheng, C. Wang, Z. Liu, Y. Fan, X. Chen, Z. Li, Z.L. Wang, Refreshable braille display system based on triboelectric nanogenerator and dielectric elastomer, Adv. Funct. Mater. (ISSN: 16163028) 31 (2021) http://dx.doi.org/10.1002/adfm.202006612.

[47] X. Ji, X. Liu, V. Cacucciolo, Y. Civet, A.E. Haitami, S. Cantin, Y. Perriard, H. Shea, Untethered feel-through haptics using 18-μ m thick dielectric elastomer actuators, Adv. Funct. Mater. (ISSN: 16163028) 31 (2021) http://dx.doi.org/10.1002/adfm.202006639.

[48] Y. Zhao, L.J. Yin, S.L. Zhong, J.W. Zha, Z.M. Dang, Review of dielectric elastomers for actuators, generators and sensors, 2020, ISSN 25143255.

[49] M. Gei, R. Springhetti, E. Bortot, Performance of soft dielectric laminated composites, Smart Mater. Struct. 22 (2013) 1–8, http://dx.doi.org/10.1088/0964-1726/22/10/104014.

[50] F. Marín, R. Ortigosa, J. Martínez-Frutos, A.J. Gil, Viscoelastic up-scaling rank-one effects in in-silico modelling of electro-active polymers, CMAME 389 (2022) 1–44, http://dx.doi.org/10.1016/j.cma.2021.114358.

[51] N. Ellmer, R. Ortigosa, J. Martínez-Frutos, R. Poya, J. Sienz, A.J. Gil, Stretch-based hyperelastic electromechanical constitutive metamodels via gradient enhanced Gaussian predictors using hierarchical structure discovery, CMAME Under Review (2025) http://dx.doi.org/10.2139/ssrn.5276388.

[52] E. Hajiesmaili, D.R. Clarke, Reconfigurable shape-morphing dielectric elastomers using spatially varying electric fields, Nat. Commun. 10 (2019) 1–8, http://dx.doi.org/10.1038/s41467-018-08094-w, URL https://www.nature.com/articles/s41467-018-08094-w.

[53] J. Martínez-Frutos, R. Ortigosa, A.J. Gil, In-silico design of electrode meso-architecture for shape morphing dielectric elastomers, JMPS 157 (2021) 104594, http://dx.doi.org/10.1016/j.jmps.2021.104594.

[54] E. Hajiesmaili, E. Khare, A. Chortos, J. Lewis, D.R. Clarke, Voltage-controlled morphing of dielectric elastomer circular sheets into conical surfaces, Extrem. Mech. Lett. 30 (2019) 100504, http://dx.doi.org/10.1016/j.eml.2019.100504.

[55] R. Ortigosa, J. Martínez-Frutos, Topology optimisation of stiffeners layout for shape-morphing of dielectric elastomers, Struct. Multidiscip. Optim. 64 (2021) 3681–3703, http://dx.doi.org/10.1007/s00158-021-03047-2.

[56] R. Ortigosa, J. Martínez-Frutos, A.J. Gil, Programming shape-morphing electroactive polymers through multi-material topology optimisation, Appl. Math. Model. 118 (2023) 346–369, http://dx.doi.org/10.1016/j.apm.2023.01.041.

[57] R. Ortigosa, J. Martínez-Frutos, Multi-resolution methods for the topology optimization of nonlinear electro-active polymers at large strains, Comput. Mech. 68 (2021) 271–293, http://dx.doi.org/10.1007/s00466-021-02030-4.

[58] R. Ortigosa, D. Ruiz, A.J. Gil, A. Donoso, J.C. Bellido, A stabilisation approach for topology optimisation of hyperelastic structures with the SIMP method, CMAME 364 (2020) 112924, http://dx.doi.org/10.1016/j.cma.2020.112924.

[59] M. PBendsoe, O. Sigmund, Topology Optimzation, Springer-Verlag, Berlin, 2003.

[60] M.Y. Wang, X. Wang, D. Guo, A level set method for structural topology optimization, CMAME 192 (2003) 227–246, http://dx.doi.org/10.1016/S0045-7825(02)00559-5.

[61] G. Allaire, F. Jouve, A.-M. Toader, Structural optimization using sensitivity analysis and a level-set method, J. Comput. Phys. 194 (2004) 363–393, http://dx.doi.org/10.1016/j.jcp.2003.09.032.

[62] M. Burger, R. Stainko, Phase-field relaxation of topology optimization with local stress constraints, J. Control. Optim. 45 (2006) 147–1466, http://dx.doi.org/10.1137/05062723X.

[63] A. Takezawa, S. Nishiwaki, M. Kitamura, Shape and topology optimization based on the phase field method and sensitivity analysis, J. Comput. Phys. 229 (2010) 2697–2718, http://dx.doi.org/10.1016/j.jcp.2009.12.017.

[64] A.T. Conn, J. Rossiter, Towards holonomic electro-elastomer actuators with six degrees of freedom, Smart Mater. Struct. 21 (2012) 035012, http://dx.doi.org/10.1088/0964-1726/21/3/035012.

[65] N. Wang, H. Guo, B. Chen, C. Cui, X. Zhang, Design of a rotary dielectric elastomer actuator using a topology optimization method based on pairs of curves, Smart Mater. Struct. 27 (2018) 055011, http://dx.doi.org/10.1088/1361-665X/aab991.

[66] F. Chen, K. Liu, Y. Wang, J. Zou, G. Gu, X. Zhu, Automatic design of soft dielectric elastomer actuators with optimal spatial electric fields, IEEE Trans. Robot. 35 (2019) 1150–1165, http://dx.doi.org/10.1109/TRO.2019.2920108.

[67] R. Ortigosa, J. Martínez-Frutos, D. Ruiz, A. Donoso, J.C. Bellido, Density-based topology optimisation considering nonlinear electromechanics, Struct. Multidiscip. Optim. 64 (2021) 257–280, http://dx.doi.org/10.1007/s00158-021-02886-3.

[68] S. Shian, K. Bertoldi, D.R. Clarke, Dielectric elastomer based "grippers" for soft robotics, Adv. Mater. 27 (2015) 6769–7009, http://dx.doi.org/10.1002/adma.201503078.

[69] G. Gonzalez, I. Roppolo, C.F. Pirri, A. Chiappone, Current and emerging trends in polymeric 3D printed microfluidic devices, 2022, ISSN 22148604.

[70] S. O'Halloran, A. Pandit, A. Heise, A. Kellett, Two-photon polymerization: Fundamentals, materials, and chemical modification strategies, 2023, ISSN 21983844.

[71] A. Bastola, Y. He, J. Im, G. Rivers, F. Wang, R. Worsley, J.S. Austin, O. Nelson-Dummett, R.D. Wildman, R. Hague, C.J. Tuck, L. Turyanska, Formulation of functional materials for inkjet printing: A pathway towards fully 3D printed electronics, 2023, ISSN 27729494.

[72] A. Bastola, L. Parry, R. Worsley, N. Ahmed, E. Lester, R. Hague, C. Tuck, Drop-on-demand 3D printing of programable magnetic composites for soft robotics, Addit. Manuf. Lett. (ISSN: 27723690) 11 (2024) http://dx.doi.org/10.1016/j.addlet.2024.100250.

[73] Y. Wu, H. Su, M. Li, H. Xing, Digital light processing-based multi-material bioprinting: Processes, applications, and perspectives, 2023, ISSN 15524965.

[74] U. Shaukat, E. Rossegger, S. Schlögl, A review of multi-material 3D printing of functional materials via vat photopolymerization, 2022, ISSN 20734360.

[75] D. Han, H. Lee, Recent advances in multi-material additive manufacturing: methods and applications, 2020, ISSN 22113398.

[76] C. Zhang, W. Wei, H. Sun, Q. Zhu, Study on the properties of different dielectric elastomers applying to actuators, Sensors Actuators A: Phys. (ISSN: 09244247) 329 (2021) http://dx.doi.org/10.1016/j.sna.2021.112806.

[77] D. Gonzalez, J. Garcia, B. Newell, Electromechanical characterization of a 3D printed dielectric material for dielectric electroactive polymer actuators, Sensors Actuators A: Phys. (ISSN: 09244247) 297 (2019) 111565, http://dx.doi.org/10.1016/j.sna.2019.111565, URL https://www.sciencedirect.com/science/article/pii/S0924424719308556.

[78] Recreus, Conductive filaflex, 2024, https://recreus.com/gb/filaments/3-filaflex-conductivo.html. (Accessed 17 December 2024).

[79] F. Zhou, M. Zhang, X. Cao, Z. Zhang, X. Chen, Y. Xiao, Y. Liang, T.W. Wong, T. Li, Z. Xu, Fabrication and modeling of dielectric elastomer soft actuator with 3D printed thermoplastic frame, Sensors Actuators A: Phys. (ISSN: 09244247) 292 (2019) 112–120, http://dx.doi.org/10.1016/j.sna.2019.02.017.

[80] P. Huang, H. Fu, M.W.M. Tan, Y. Jiang, P.S. Lee, Digital light processing 3D-printed multilayer dielectric elastomer actuator for vibrotactile device, Adv. Mater. Technol. (ISSN: 2365709X) 9 (2024) http://dx.doi.org/10.1002/admt.202301642.

[81] I. Liashenko, J. Rosell-Llompart, A. Cabot, Ultrafast 3D printing with sub-micrometer features using electrostatic jet deflection, Nat. Commun. (ISSN: 20411723) 11 (2020) http://dx.doi.org/10.1038/s41467-020-14557-w.

[82] L. Jiang, Y. Wang, X. Wang, F. Ning, S. Wen, Y. Zhou, S. Chen, A. Betts, S. Jerrams, F.L. Zhou, Electrohydrodynamic printing of a dielectric elastomer actuator and its application in tunable lenses, Compos. Part A: Appl. Sci. Manuf. (ISSN: 1359835X) 147 (2021) http://dx.doi.org/10.1016/j.compositesa.2021.106461.

[83] A. Chortos, E. Hajiesmaili, J. Morales, D.R. Clarke, J.A. Lewis, 3D printing of interdigitated dielectric elastomer actuators, Adv. Funct. Mater. (ISSN: 16163028) 30 (1) (2020) 1–10, http://dx.doi.org/10.1002/adfm.201907375, URL https://onlinelibrary.wiley.com/doi/full/10.1002/adfm.201907375.

[84] A. Malas, E. Saleh, M.d.C. Giménez-López, G.A. Rance, T. Helps, M. Taghavi, J.M. Rossiter, C.J. Tuck, I.A. Ashcroft, R.D. Goodridge, Reactive jetting of high viscosity nanocomposites for dielectric elastomer actuation, Adv. Mater. Technol. (ISSN: 2365709X) 7 (6) (2022) 1–11, http://dx.doi.org/10.1002/admt.202101111.

[85] N.M. Larson, J. Mueller, A. Chortos, Z.S. Davidson, D.R. Clarke, J.A. Lewis, Rotational multimaterial printing of filaments with subvoxel control, Nature (ISSN: 14764687) 613 (7945) (2023) 682–688, http://dx.doi.org/10.1038/s41586-022-05490-7.

[86] P.M. Danner, T. Pleij, G. Siqueira, A.V. Bayles, T.R. Venkatesan, J. Vermant, D.M. Opris, Polysiloxane inks for multimaterial 3d printing of high-permittivity dielectric elastomers, Adv. Funct. Mater. (ISSN: 16163028) 34 (2024) http://dx.doi.org/10.1002/adfm.202313167.

[87] I. Raguž, M. Berer, M. Fleisch, C. Holzer, J. Brancart, B. Vanderborght, S. Schlögl, Soft dielectric actuator produced by multi-material fused filament fabrication 3D printing, Polym. Adv. Technol. (ISSN: 10991581) 34 (2023) 1967–1978, http://dx.doi.org/10.1002/pat.6024.

[88] S.G. Uzel, R.D. Weeks, M. Eriksson, D. Kokkinis, J.A. Lewis, Multimaterial multinozzle adaptive 3D printing of soft materials, Adv. Mater. Technol. (ISSN: 2365709X) 7 (8) (2022) 1–10, http://dx.doi.org/10.1002/admt.202101710, URL https://onlinelibrary.wiley.com/doi/full/10.1002/admt.202101710.

[89] G. Kofod, H. Stoyanov, R. Gerhard, Multilayer coaxial fiber dielectric elastomers for actuation and sensing, Appl. Phys. A: Mater. Sci. Process. (ISSN: 09478396) 102 (3) (2011) 577–581, http://dx.doi.org/10.1007/s00339-010-6066-5.

[90] Y. Zhu, N. Liu, Z. Chen, H. He, Z. Wang, Z. Gu, Y. Chen, J. Mao, Y. Luo, Y. He, 3D-printed high-frequency dielectric elastomer actuator toward insect-scale ultrafast soft robot, ACS Mater. Lett. (ISSN: 26394979) 5 (2023) 704–714, http://dx.doi.org/10.1021/acsmaterialslett.2c00991.

[91] J. Yi, F. Babick, C. Strobel, S. Rosset, L. Ciarella, D. Borin, K. Wilson, I. Anderson, A. Richter, E.F. Henke, Characterizations and inkjet printing of carbon black electrodes for dielectric elastomer actuators, ACS Appl. Mater. Interfaces (ISSN: 19448252) 15 (2023) 41992–42003, http://dx.doi.org/10.1021/acsami.3c05444.

[92] Z. Lyu, J.J. Koh, G.J.H. Lim, D. Zhang, T. Xiong, L. Zhang, S. Liu, J. Duan, J. Ding, J. Wang, J. Wang, Y. Chen, C. He, Direct ink writing of programmable functional silicone-based composites for 4D printing applications, Interdiscip. Mater. (ISSN: 2767-441X) 1 (4) (2022) 507–516, http://dx.doi.org/10.1002/idm2.12027.

[93] N.A. Che Nasir, M.S. Saharudin, W.N. Wan Jusoh, O.S. Kooi, Effect of nanofillers on the mechanical properties of epoxy nanocomposites, Adv. Struct. Mater. (ISSN: 18698441) 167 (1) (2022) 199–208, http://dx.doi.org/10.1007/978-3-030-89988-2_15.

[94] M. Mehnert, J. Faber, M. Hossain, S.A. Chester, P. Steinmann, Experimental and numerical investigation of the electro-mechanical response of particle filled elastomers - part I: Experimental investigations, Eur. J. Mech. A Solids (ISSN: 09977538) 96 (2022) http://dx.doi.org/10.1016/j.euromechsol.2022.104651.

[95] A. Kumar, K. Patra, M. Hossain, Silicone composites cured under a high electric field: an electromechanical experimental study, Polym. Compos. (ISSN: 15480569) 42 (2021) 914–930, http://dx.doi.org/10.1002/pc.25875.

[96] S. Wu, Z. Wang, Y. Cai, Y. Chen, Z. Xian, Y. Luo, H. You, C. Sun, The research on nozzles for microscale printing of high viscosity pastes containing micron-sized particles, J. Manuf. Process. (ISSN: 15266125) 125 (2024) 226–238, http://dx.doi.org/10.1016/j.jmapro.2024.07.030.

[97] R. Chen, A. Bratten, J. Rittenhouse, T. Huang, W. Jia, M.C. Leu, H. Wen, Additive manufacturing of complexly shaped SiC with high density via extrusion-based technique – effects of slurry thixotropic behavior and 3D printing parameters, Ceram. Int. (ISSN: 02728842) 48 (2022) 28444–28454, http://dx.doi.org/10.1016/j.ceramint.2022.06.158.

[98] Q. Liu, N. Zhang, W. Wei, X. Hu, Y. Tan, Y. Yu, Y. Deng, C. Bi, L. Zhang, H. Zhang, Assessing the dynamic extrusion-based 3D printing process for power-law fluid using numerical simulation, J. Food Eng. (ISSN: 02608774) 275 (2020) http://dx.doi.org/10.1016/j.jfoodeng.2019.109861.

[99] A. Marnot, A. Dobbs, B. Brettmann, Material extrusion additive manufacturing of dense pastes consisting of macroscopic particles, MRS Commun. (ISSN: 21596867) 12 (2022) 483–494, http://dx.doi.org/10.1557/s43579-022-00209-1.

[100] Y. Shi, E. Askounis, R. Plamthottam, T. Libby, Z. Peng, K. Youssef, J. Pu, R. Pelrine, Q. Pei, A processable, high-performance dielectric elastomer and multilayering process, Science (ISSN: 0036-8075) 377 (2022) 228–232, http://dx.doi.org/10.1126/science.abn0099, URL https://www.science.org/doi/10.1126/science.abn0099.

[101] W. Feng, L. Sun, Z. Jin, L. Chen, Y. Liu, H. Xu, C. Wang, A large-strain and ultrahigh energy density dielectric elastomer for fast moving soft robot, Nat. Commun. (ISSN: 20411723) 15 (2024) http://dx.doi.org/10.1038/s41467-024-48243-y.

[102] A. Poulin, S. Rosset, H.R. Shea, Printing low-voltage dielectric elastomer actuators, Appl. Phys. Lett. (ISSN: 00036951) 107 (2015) http://dx.doi.org/10.1063/1.4937735.

[103] S. Park, A. Goldin, J. Rivas-Davila, Miniature high-voltage DC-dc power converters for space and micro-robotic applications, in: Miniature High-Voltage DC-DC Power Converters for Space and Micro-Robotic Applications, IEEE, Baltimore, MD, USA, ISBN: 9781728103952, 2019, http://dx.doi.org/10.1109/ECCE.2019.8913249, URL https://ieeexplore.ieee.org/document/8913249.

[104] Bambu labs, 2025, https://uk.store.bambulab.com/products/ams-multicolor-printing?skr=yes. (Accessed 06 January 2025).

[105] Creality, 2025, https://store.creality.com/products/cfs-creality-filament-system. (Accessed 06 January 2025).

[106] SYGNIS soft gripper, 2025, https://diw3d.com/applications/soft-gripper-3d-printed-soft-robotics/. (Accessed 06 January 2025).

[107] Cellink, 2025, https://www.cellink.com/bioprinting/bio-x6-3d-bioprinter/. (Accessed 09 January 2025).

[108] Inkbit, 2025, https://inkbit3d.com/technology/. (Accessed 14 January 2025).

[109] T.J. Buchner, S. Rogler, S. Weirich, Y. Armati, B.G. Cangan, J. Ramos, S.T. Twiddy, D.M. Marini, A. Weber, D. Chen, G. Ellson, J. Jacob, W. Zengerle, D. Katalichenko, C. Keny, W. Matusik, R.K. Katzschmann, Vision-controlled jetting for composite systems and robots, Nature (ISSN: 14764687) 623 (2023) 522–530, http://dx.doi.org/10.1038/s41586-023-06684-3.

[110] D.J. Roach, C.M. Hamel, C.K. Dunn, M.V. Johnson, X. Kuang, H.J. Qi, The m4 3D printer: A multi-material multi-method additive manufacturing platform for future 3D printed structures, Addit. Manuf. (ISSN: 22148604) 29 (2019) http://dx.doi.org/10.1016/j.addma.2019.100819.

[111] Regenhu, 2025, https://www.regenhu.com/3dbioprinting-solutions/r-gen-100-3dbioprinter/#versatile-configuration. (Accessed 08 January 2025).

[112] Bioplotter, 2025, https://health.desktopmetal.com/3d-printers/3d-bioplotter/. (Accessed 14 January 2025).

[113] J. Whitehead, H. Lipson, Multi-process printing method combining powder and resin based additive manufacturing, Addit. Manuf. Lett. (ISSN: 27723690) 3 (2022) http://dx.doi.org/10.1016/j.addlet.2022.100062.

[114] X. Peng, X. Kuang, D.J. Roach, Y. Wang, C.M. Hamel, C. Lu, H.J. Qi, Integrating digital light processing with direct ink writing for hybrid 3D printing of functional structures and devices, Addit. Manuf. (ISSN: 22148604) 40 (2021) http://dx.doi.org/10.1016/j.addma.2021.101911.

[115] M.S. Aydin, N. Marek, T. Luciani, S. Mohamed-Ahmed, B. Lund, C. Gjerde, K. Mustafa, S. Suliman, A. Rashad, Impact of porosity and stiffness of 3D printed polycaprolactone scaffolds on osteogenic differentiation of human mesenchymal stromal cells and activation of dendritic cells, ACS Biomater. Sci. Eng. (ISSN: 23739878) (2024) http://dx.doi.org/10.1021/acsbiomaterials.4c01108.